

Award Number: 07HQAG0025

**CONTINUOUS BROADBAND MONITORING OF CRUSTAL DEFORMATION
NEAR ACTIVE FAULTS IN SOUTHERN CALIFORNIA**

Start and End Dates: 3/1/2007 to 2/28/2010

Final Technical Report, May 31, 2010

Duncan Carr Agnew

Institute of Geophysics and Planetary Physics
Scripps Institution of Oceanography
University of California, San Diego
La Jolla, CA 92093-0225
(858) 534-2590 (FAX 534-5332); dagnew@ucsd.edu

Frank K. Wyatt

Institute of Geophysics and Planetary Physics
Scripps Institution of Oceanography
University of California, San Diego
La Jolla, CA 92093-0225
(858) 534-2411 (FAX 534-5332); fwyatt@ucsd.edu

Award Number: 07HQAG0025

CONTINUOUS BROADBAND MONITORING OF CRUSTAL DEFORMATION NEAR ACTIVE FAULTS IN SOUTHERN CALIFORNIA

Duncan Carr Agnew
Frank K. Wyatt

Abstract

This grant provides partial support for the operation of two facilities that measure strain changes in Southern California: Piñon Flat Observatory (PFO), between the San Jacinto and San Andreas faults, and at Durmid Hill (DHL), near the southern end of the San Andreas fault—and effectively within the fault zone. The USGS-sponsored instruments at these locations—a single longbase strainmeter at DHL, and three strainmeters and one tiltmeter at PFO—measure crustal deformation in Southern California for periods from seconds to years. In the period covered by this report we have observed several significant strain events.

Report

1. Introduction

This grant helps to support the operation of two facilities for the continuous measurement of strain changes in Southern California: Piñon Flat Observatory (PFO), between the San Jacinto and San Andreas faults, and at Durmid Hill (DHL), near the southern end of the San Andreas fault—and effectively within the fault zone. Other operational support for PFO is provided by SCEC and for DHL by the Plate Boundary Observatory project, with matching funds for both sites from Scripps Institution of Oceanography.

Long-Base Instruments Supported

Site	Component	Local End		Remote End		Length (m)
		Lat	Long	Lat	Long	
PFO	NS	-116.460182	33.612370	-116.460213	33.605770	732
PFO	EW	-116.451797	33.612316	-116.459679	33.612370	716
PFO	NWSE	-116.459572	33.612198	-116.454033	33.607521	730
PFO	EW tilt	-116.45847	33.61214	-116.45183	33.61049	505
DHL	N5°E	-115.788235	33.389865	-115.788665	33.394577	524

The instruments at these locations (two longbase strainmeters at DHL, three strainmeters and two tiltmeters at PFO) measure crustal deformation in Southern California for periods from seconds to years. By recording strain over this wide range of frequencies these measurements provide a nearly unique bridge between seismology and geodesy that is rarely available. At PFO, intercomparison of results from many types of sensors gives the best records available. An accurate record of strain and tilt changes in the area near the observatories provides a better understanding of the mechanics of faulting, useful both for studies of the seismic cycle in Southern California and for comparison with other types of measurements of crustal deformation.

This award provides funding primarily for operation of the observatories including support for power distribution, data recording, preliminary data-processing, and data distribution: all basic activities, but all needed if the observatories are to operate and provide recordings. (For DHL—which now has two longbase strainmeters—the operational costs for the new component, DHM, are covered exclusively by PBO.) Part of the support is to cover the creation of well-edited versions of the data, under the supervision of the PIs.

In the absence of a significant geophysical event, it is in the nature of this kind of data collection that there may not be something new to report in the data every year; however, even without events, the accumulation of data can reveal new information. This report gives examples of both kinds of results.

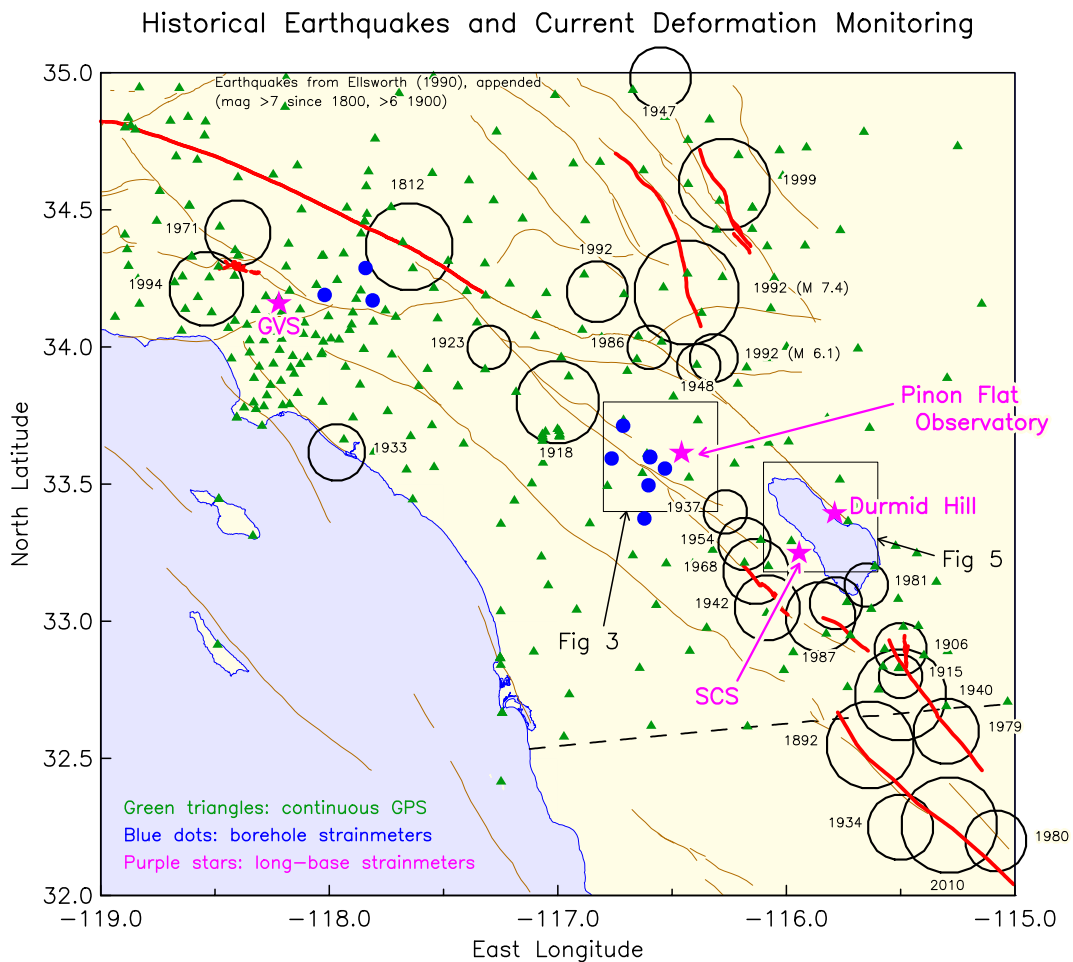


Figure 1

2. Background on Strainmeter Sites

Figure 1 shows where PFO and DHL are relative to areas of strain release: that is, large historic earthquakes, and also relative to other deformation monitoring: continuous GPS (SCIGN and the PBO) and borehole strain (USGS and PBO). Figure 2 shows areas of strain accumulation: the estimated shear strain rate inferred from the geodetic velocities from the SCEC Crustal Motion Map (CMM). Both observatories are in areas with considerable strain change, either way.

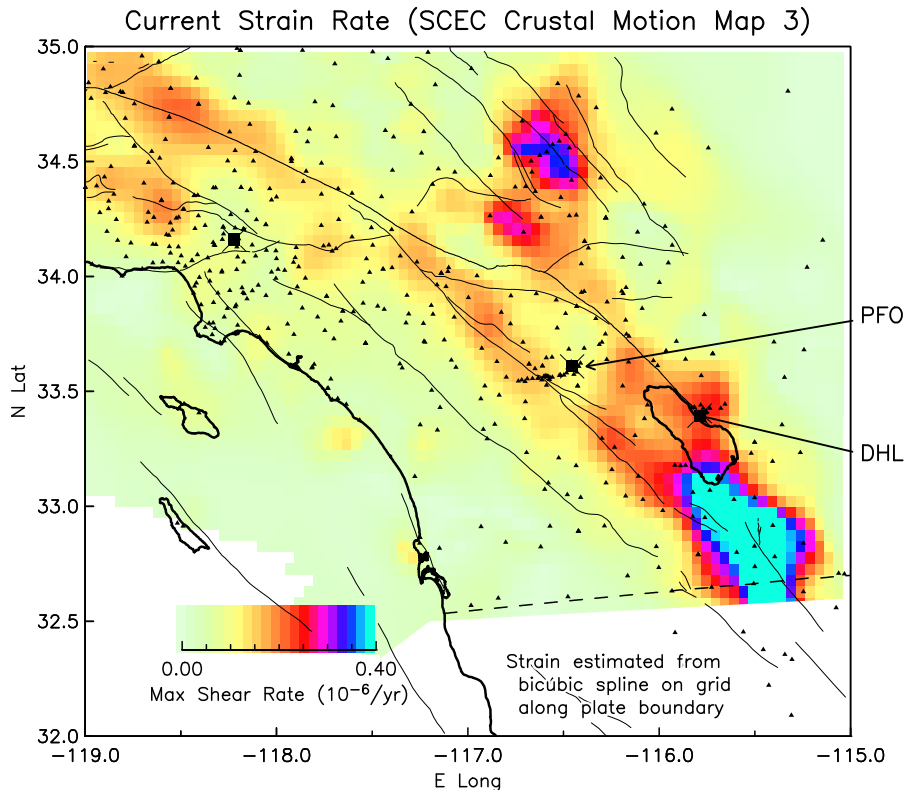


Figure 2

2.1. PFO: Local Seismotectonics and Deformation, and Site History

Figure 3 shows an expanded view around PFO, including velocities of geodetic sites relative to PFO, from the SCEC Crustal Motion Map. As expected in this region of strike-slip faults, the predominant motion is simple shear; the local velocity gradient of $2.4 \times 10^{-7} \text{ yr}^{-1}$, agrees with the expected deformation from the two nearest active faults. The closest is the San Jacinto fault zone, 14 km SW of PFO. The geological slip rate is about 10 mm/yr; paleoseismic data show six surface ruptures since about AD 1000 (average interval 150-200 yr); the last event was in about AD 1760 (T. Rockwell, pers. commun.), implying a slip deficit of at least 3 m. That this section of the fault lacked a historic earthquake, and so could be regarded as a seismic “slip gap” was one reason why PFO was located where it was. This reasoning remains valid, and there are new reasons to find this fault interesting: the section nearest PFO produced nonvolcanic tremor in response to the 2002 Denali earthquake (Gomberg *et al.* 2008) and the 2009 Gulf of California earthquake (Brown *et al.* 2009), and accelerated aseismic strains following the 2005 Anza earthquake.

PFO is also relatively close to the San Andreas fault zone (25 km NE), and again this nearby section is also “overdue”, with an accumulated slip deficit of 8 m since the last large slip event around AD 1700; the average recurrence time is about 200 years.

Figure 4 shows a site plan for PFO, named for Pinyon Flat, a large flat area of shallowly weathered granodiorite. (There is about 3 m of decomposed material underlain by about 20 m of competent grus, grading into unweathered and relatively unfractured material below about 70 m; Fletcher *et al.*, 1990; Radzevicius and Pavlis, 1999.)

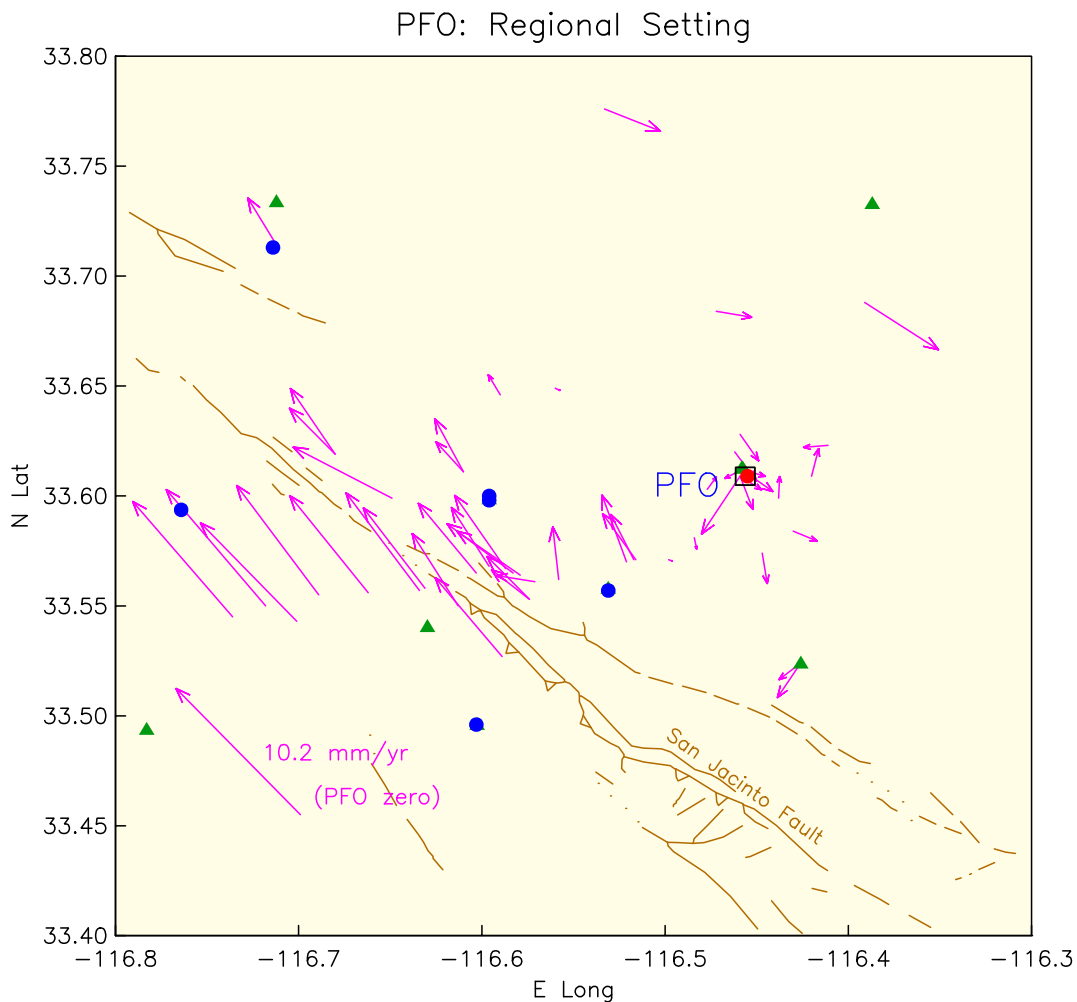


Figure 3

Observations at PFO began in the early 1970's, with the original construction of the three longbase strainmeters. Between 1979 and 1990 we made many improvements (notably in anchoring the ends of some of the instruments) added additional systems (such as borehole sensors and longbase tiltmeters) and performed a number of tests to compare different measurement methods. Since 1991 a major part of our work at PFO has been making the operations more reliable and less costly. Some of this ongoing improvement is done within the limits of operational budgets; we also have made instrument upgrades and improvements (Section 2.5), with support from non-operational funds. A recent example (supported by NSF) is the complete reconstruction of the EW long-base strainmeter (2002 through 2003) to have optical anchors.

2.2. DHL: Local Seismotectonics and Deformation, and Site History

The southern termination of the San Andreas fault is marked by changes in both surface appearance and seismicity. The surface trace, which is extremely obvious as far south as Salt Creek (**Figure 2**), becomes less obvious further south, and is not visible at Bombay Beach. At Bombay Beach the seismicity also changes—or, more properly, the seismicity appears, since to the north the San Andreas is nearly aseismic, while to the south, the seismicity forms a broad zone trending about 15° more southerly than the

Piñon Flat Observatory

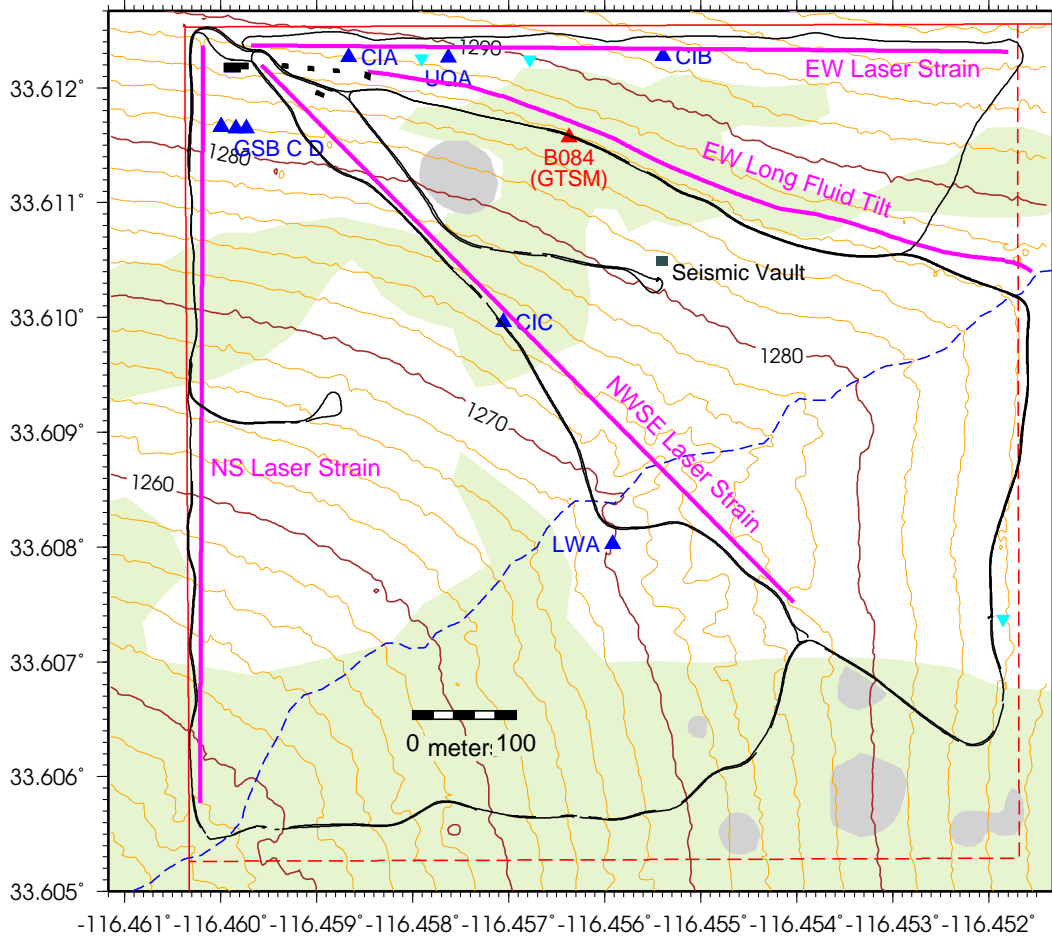


Figure 4

SAF. Relocated epicenters (Shearer *et al.* 2006) show numerous streaks of seismicity roughly orthogonal to the trend of the zone, suggesting pervasive cross-faulting, which is present in other areas nearby (Hudnut *et al.* 1989). At the southern end of the Salton Sea this pattern is obscured by the very large number of earthquakes induced by local geothermal power extraction, though even in this region precisely-located seismicity delineates faults along and across the trend of the zone (Lohman and McGuire 2007). This broad pattern of seismicity extends further to the south, forming the Brawley Seismic Zone (BSZ), which eventually merges into earthquakes that are more clearly lineated along the Imperial Fault. (The term “Brawley Seismic Zone” is usually applied to the whole trend from Bombay Beach south to the Imperial fault; for clarity we call that part of the trend north of the volcanic centers associated with the geothermal plants, the Salton Seismic Zone.) Given the obliquity of the BSZ to the local direction of plate motion, it is reasonable to take this to be a region of transensional motion, combining strike-slip with some amount of spreading.

Of course, this section of the San Andreas fault is of great interest because it is, so far as is known, the “most overdue” for a great earthquake. Current evidence suggests that the last large slip event was around AD 1690. Given a slip rate of 24 mm/yr (Meade and Hager 2005, McCaffrey 2005), there is an accumulated slip deficit of 8 m. The seismicity (even to low magnitudes) of this part of the San Andreas

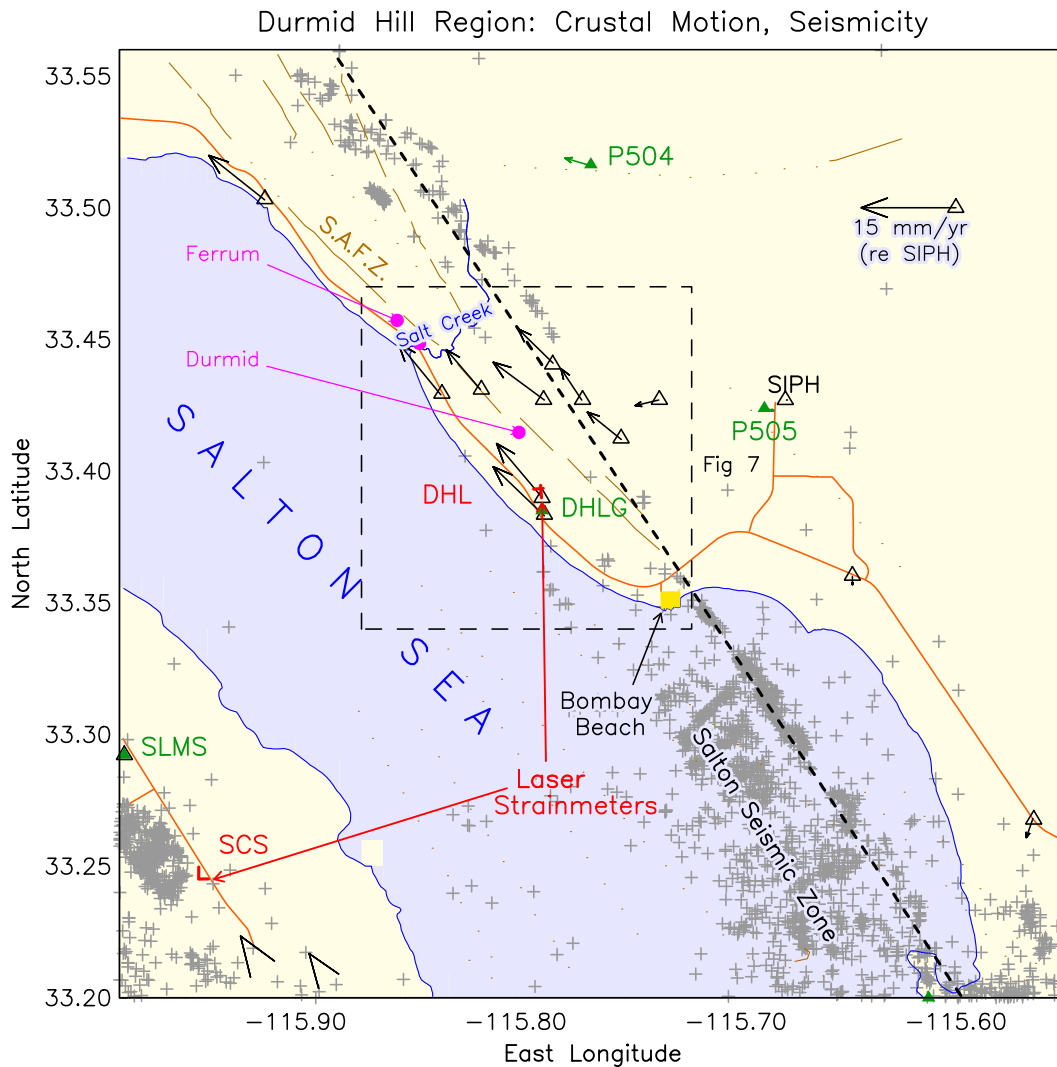


Figure 5. The San Andreas Fault (brown) and its transition into the Brawley (Salton) Seismic Zone, at Bombay Beach. Black and green arrows and triangles are GPS stations and interseismic velocities (green for continuous GPS). Red shows the USGS and PBO laser strainmeters. Small filled triangles are other points with existing GPS data. Seismicity is for 1981-2005, magnitude 1 and above, from the LSH catalog of relocated earthquakes, 1981-2005 (Shearer *et al.* 2007).

is very low, though the geomorphic expression of the fault is extremely clear. Geodetic measurements show nearly pure shear; from Salt Creek north there have been small amounts of creep (1-2 mm/yr), along with creep triggered at the times of large earthquakes (Allen *et al.* 1972; Louie *et al.* 1985; Williams *et al.* 1988; Sieh and Williams 1990; Lyons and Sandwell 2003). The most recent examination of deformation in this region (Fialko 2006) used InSAR and GPS data to conclude that this section of the SAF had a current slip rate around 25 mm/yr, though fitting the data required that the Salton trough region have a much higher shear modulus than the area to the east, a somewhat counterintuitive result; see also Fay and Humphreys (2005). Comparisons of EDM and GPS (Johnson *et al.* 1994; Anderson *et al.* 2003) show that the rates of deformation have been steady over the last several decades, with the exception of local deformations related to the geothermal plants at the southern end of the Salton Seismic Zone; these results also show that this region is undergoing local dilatation, something not easily explained by dislocation

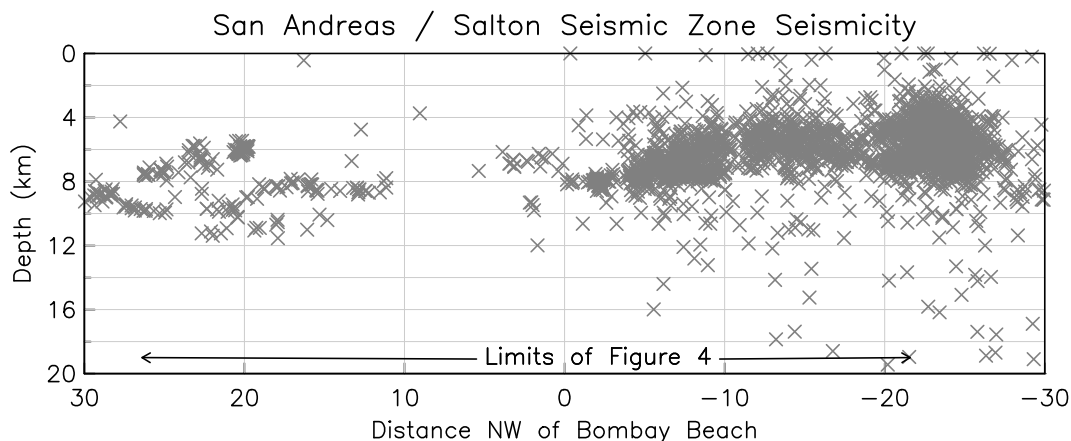


Figure 6: Cross-section of seismicity within 5 km of the Brawley (Salton) Seismic Zone and its northward extrapolation (dashed line in **Figure 5**). The cluster of earthquakes on the left are a lineation of seismicity NE of the trace of the San Andreas.

models.

The southernmost section of the fault runs through a large, gentle topographic uplift known as Durmid Hill (**Figure 7**); the local geology (Babcock 1969; Bürgmann 1991) is interbedded claystones and siltstones, much deformed and only weakly cemented together. In 1988 this section of the San Andreas was identified as having the next-highest probability (after Parkfield) of producing an earthquake in the next 30 years; a subsequent study (Jones *et al.* 1991) suggested that more monitoring was needed. This led to the construction of a north-south long-base strainmeter, which has been operating since late 1994. This site was also chosen for the first of the PBO long-base strainmeters, built at right angles to the original north-south instrument to provide fuller coverage (including independent corroboration of aseismic events); this has been operating since May 2005. A continuous GPS site was installed next to the DHL strainmeter in 1996, and a site across the Salton Sea in 1999. More recently, the PBO has installed a number of additional continuous GPS sites in 2005 and 2006; and also a second set of laser strainmeters at Salton City (SCS, on the west side of the Salton Sea), operating since October 2006. Creep measurements along this section of the fault were begun in 1970 by Caltech, ending in the early 1990's; Prof. Roger Bilham installed new creepmeters in 2004, and these are currently in operation (Bilham *et al.* 2004).

2.3. Other Longbase Strainmeter Installations

The first DHL installation, which allowed us to apply newer systems, led us towards construction of additional sensors elsewhere. The SCIGN network, while primarily devoted to GPS, also supported construction of a single-component instrument in Glendale, at the northern edge of the Los Angeles basin: site GVS, also shown in **Figure 1**. This instrument has operated since fall 2002. Initially, SCIGN provided operational support; subsequently, NSF has done so as part of their support of existing geodetic networks relevant to the EarthScope project: this strainmeter is now part of the Plate Boundary Observatory (PBO). (NSF has not supported PBO operations since 1993, and not been involved in support for DHL).

At the same time as GVS was built, we were building, with DOE funds, a strainmeter (YMS) in the exploratory tunnel at Yucca Mountain, Nevada; this was part of the characterization of this location for radioactive waste disposal. This instrument also began operation in fall 2002; in early 2007, in response to substantial decreases in DOE funding, the tunnel was closed, and this instrument shut down. Because

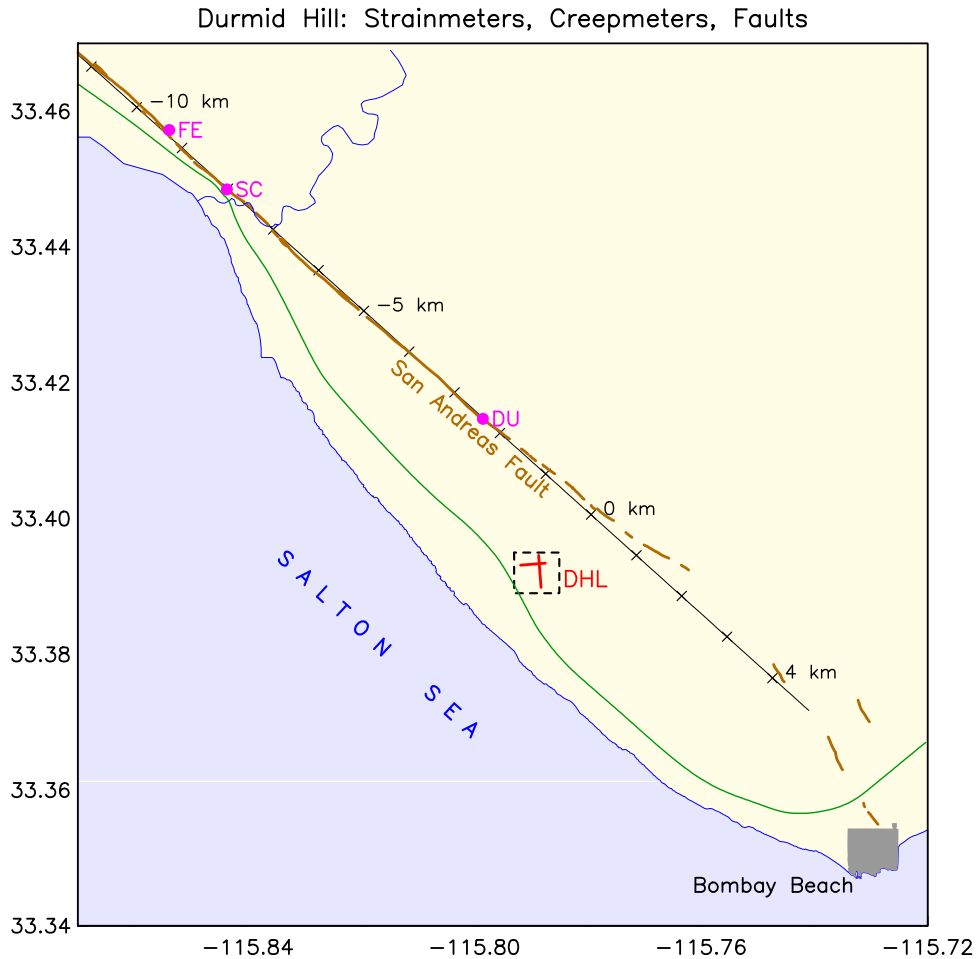


Figure 7: Detail of the Durmid Hill region. Purple circles are locations of creepmeters; the scale running along the fault is discussed in Section 3.1.1.1. Green is railway line. **Figure 8** shows the site details.

tunnel access was limited, DOE funds supported the development of remote control systems; we have since installed these into all the earlier instruments as funding has allowed.

The PBO plan included five new laser strainmeters (PBO construction funds could only be used for new installations). The first PBO LSM was the second component at DHL, mentioned above. The second and third instruments are at a site (SCS) directly across the Salton Trough from DHL (**Figure 5**) to provide additional data from the Salton Trough; these began operation in September 2006. The fourth and fifth systems were installed close to the San Andreas, in Cholame (just south of Parkfield), and began operation in August 2008.

3. Recent Strainmeter Measurements of Earthquake-Related Phenomena

We now show what the instruments at PFO and DHL are capable of, by providing examples of specific cases. As appropriate, we include comparisons with other deformation sensors.

Durmid Hill Facility

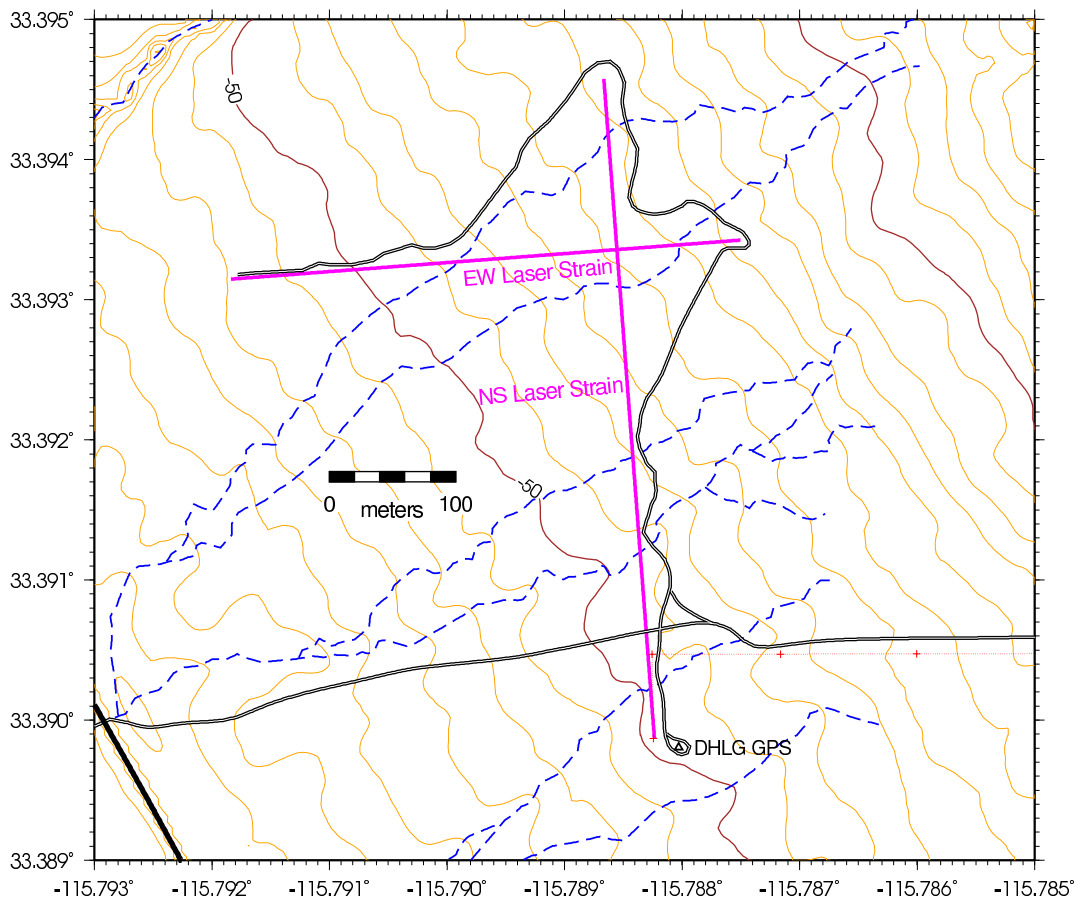


Figure 8

3.1. Long-term Strain Changes at DHL

Figure 9 shows the complete dataset from the two fully-anchored strainmeters at DHL. The (nearly) NS instrument (the one supported by this request) has a long-term rate of $-0.22 \mu\epsilon/\text{yr}$, comparable to strain rates estimated by interpolating GPS station velocities; so we conclude that this strainmeter is recording the secular strain; we believe the same of the newer PBO instrument, although its higher rate implies that there is some amount of dilatation at this site. Parts of the NS strain record show an annual cycle, with an amplitude of $35 \text{ n}\epsilon$; and a phase of 37° relative to January 1. (The local air temperature has an annual cycle of 10.7°C , phase -199.8° .) We do not yet know whether this cycle (which is only sometimes apparent) comes from thermoelastic deformation, or (quite possibly) incomplete correction of end-motion by the fiber anchors; certainly, compared to any other near-surface strain record the annual cycle is small.

Figure 10 focuses on the NS instrument for 4 years, and for context shows local seismicity, creep measured at Ferrum (data provided by Dr. Roger Bilham with NEHRP funding), and motion over a 10-km GPS baseline from DHL across the San Andreas Fault (see below).

These data show several interesting combinations of events and non-events: we see several aseismic strain events. Some of these coincide with creep signals, implying widespread slippage (over at least 10 km of the fault); others do not, and there are also creep events unaccompanied by aseismic strain.

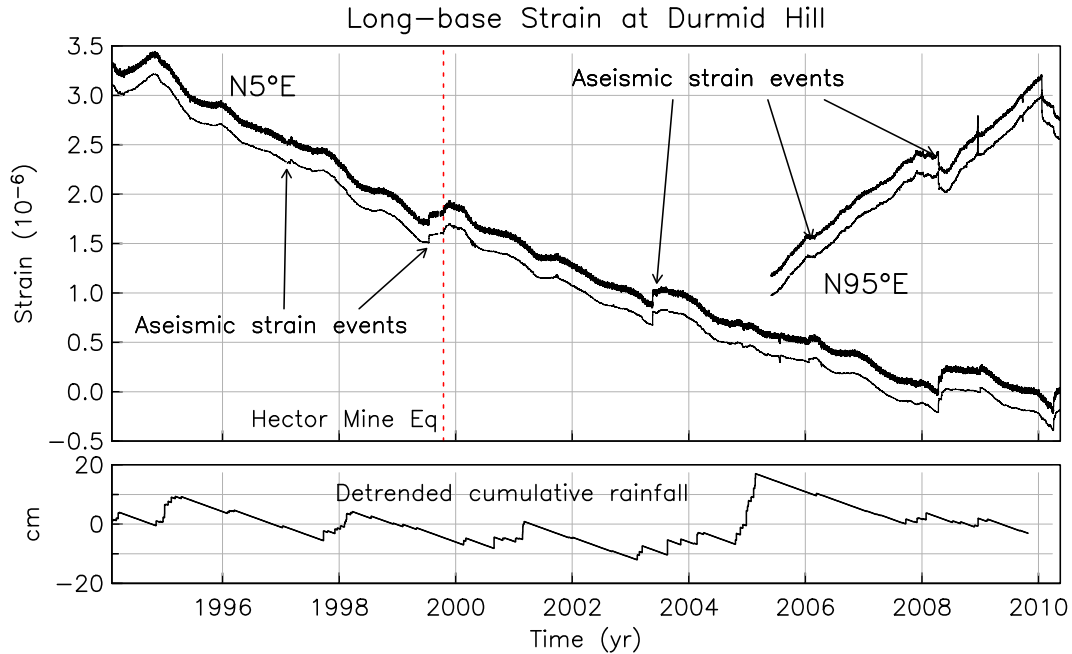


Figure 9

These last few years also included a seismic swarm, in early 2009, that caused serious concern about short-term hazard. We now discuss these in more detail.

3.2. 2008: Transients on the Southern San Andreas Fault

On the creeping section of the San Andreas fault between Parkfield and Hollister, it has been known for some time that creep at the surface often occurs in “events” with relatively rapid slip; see, for example, Gouly and Gilman (1978), Evans *et al.* (1981) and Wesson (1988). Near San Juan Bautista, several creep events between 1992 and 1998 have been associated with large aseismic strain changes, assumed to be caused by slip on relatively shallow portions of the San Andreas fault (Gladwin *et al.* 1994; Linde *et al.* 1996; Uhrhammer *et al.* 1999).

The southernmost San Andreas has small amounts of ongoing creep, and creep events triggered by large local earthquakes. The laser strainmeters at Durmid Hill (DHL) have detected a number of rapid aseismic strain changes which we believe are caused by local creep events. The first of these was observed in early 1997, though only on the one instrument then operating.

The first unequivocal records of rapid aseismic strain change at DHL were in 1999; “unequivocal” because at that time we were operating, with NSF support, a second long-base instrument, installed temporarily to measure earth tides. As these systems shared nothing except the datalogger and line power, we were confident that these events were not instrumental artefacts. Unfortunately there were no creepmeter measurements on the San Andreas fault in this area during the times of these events; a field check for cracking along the fault trace showed no clear evidence of surface fault slip. InSAR data for this segment of the fault (D. Sandwell, pers. commun.) suggests ongoing creep, but also indicates that this creep stops somewhat north of the DHL site. Buried slip of the amount we infer would not produce a measurable InSAR signal. These earlier aseismic changes clustered around the time of the 1999 Hector Mine earthquake, ending with a large strain change associated with the shaking from this shock. We also observed an additional slow event in mid-2003 and two more in early 2006.

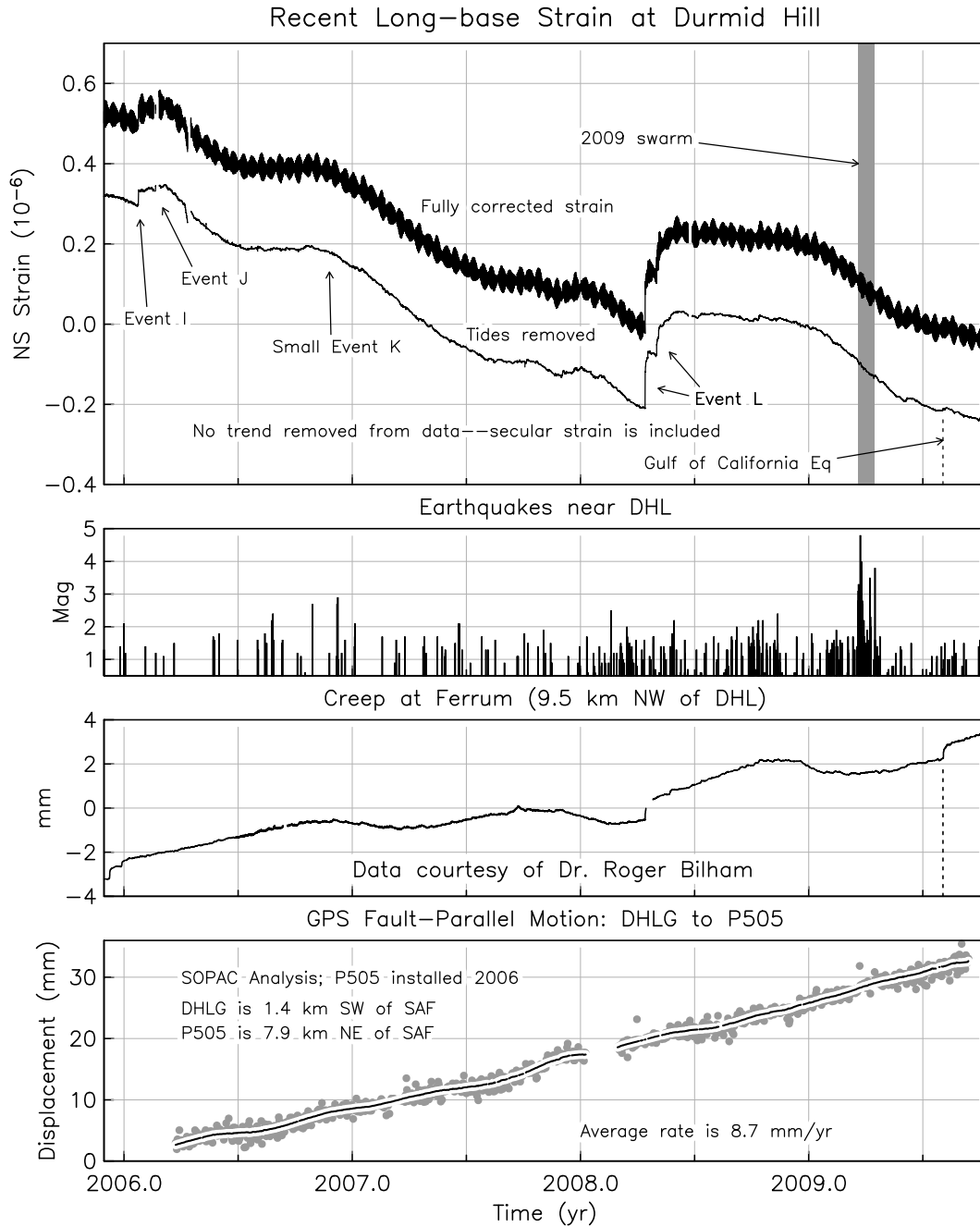


Figure 10

Figure 11 shows 2.4 years of data from some of the sensors along the fault, to the end of May, 2008. The top panel shows the long-term records from the two laser strainmeters at DHL. The long-term rate on the NS instrument is $-0.31 \mu\epsilon/\text{yr}$; the new EW system shows a rate of $0.49 \mu\epsilon/\text{yr}$ (both instruments are actually 5° counterclockwise to the directions given, to be at 45° to the local fault strike). These rates are consistent with the shear expected from a dislocation model, though they, like the geodetic results, require a local dilatation as well. The next panel shows data from the University of Colorado creepmeters (Bilham *et al* 2004), whose locations are shown in **Figure 7** (FE, SC [offscale], and DU); the FE and DU records have been corrected for short-term temperature effects, but the annual cycle has not

been removed. Both instruments show ongoing creep at rates of 1-2 mm/yr, with some left-lateral creep at times of heavy rains (rain is shown in the bottom panel). The Durmid creepmeter shows two creep events in early 2006; and both creepmeters show an abrupt signal beginning on 2008:104 (R. Bilham, pers. commun.), which was also very clear on the strainmeters, and which we describe in the next section.

As another measure of long-term deformation, and to look for any very recent changes, we processed GPS data from the 5 stations (PBO and SCIGN) closest to DHL, starting in early 2006 when the site at P505 (**Figure 5**) began producing data; such a local network is largely immune to various common-mode noise sources. The third and fourth panels from the top of **Figure 11** show two of the results. Relative to P505 (which moves only 6 mm/yr in a North-America reference frame), DHLG moves 8.2 mm/yr fault-parallel and -0.8 mm/yr fault-normal, with no obvious fluctuations. The baseline from P505 to SLMS (across the Salton Sea) has only 5 mm/yr more fault-parallel motion. However, the line from P505 to P504, which is entirely on the east side of the San Andreas, shows an apparent transient beginning sometime in the summer of 2007. It is not clear what to make of this; while it begins before the rains of late 2007, there does appear to be an annual cycle present in these data. Interestingly, this GPS transient approximately coincides with a change in the long-term rate of strain on the DHL EW strainmeter seen in late summer; we observed a similar, temporary, rate decrease at the start of 2006, which was also coincident with two aseismic slip events. Since the strainmeter data have been unaffected by rainfall at other times, we are fairly confident that the 2007 change in rate was not caused by the summer rains.

As the right-hand side of **Figure 11** shows, we have seen periods of clustering of creep events. Since creepmeter data was available for this period, we can say that these events are indeed correlated with fault creep; what is surprising is that the slip involved must extend as far south as the strainmeters (for reasons to be discussed below) and as far north as the Ferrum creepmeter, a distance of over 10 km.

The top panel of **Figure 12** shows the strainmeter data for these periods of activity, at two expanded time scales: at the top, for the few days involved in each episode; and below this, for some of the few-minute intervals that contain the larger creep events. These records give very high resolution, both in strain and in time, of these aseismic strain changes; in terms of time resolution, much finer than the data collected by Gouly and Gilman (1978), King *et al.* (1975), Linde *et al.* (1996) or Uhrhammer *et al.* (1999).

What these detailed records show is that these individual events are neither similar nor simple: while coarse temporal sampling would make them look like steps, a finer resolution shows a variety of behaviors. As described in the next section, this range of waveforms can be used to explore the spatial and temporal behavior of these events, which may serve as analogs to deeper slip events that occur when sliding is neither unstable (leading to earthquakes) or completely stable (leading to steady slip). Such episodic slip has been observed in various “slow earthquakes” at subduction zones (Ide *et al.* 2007; Shelly *et al.* 2007); the strainmeter records provide nearfield data that is not available for deeper slip episodes.

3.2.1. Source-Time Functions for Slow Slip Events

Because the strainmeter data are observed close to the source, the “near-field” term in the elastodynamic equations dominates; since this behaves quasi-statically, an inversion for source properties can be much more direct. The first step is to get the Green function for observed strain given slip at a point on the fault plane. **Figure 13** shows this computed for an elastic halfspace; the coordinate system is that used in **Figure 7**. Naturally, the response is largest for slip closest to the strainmeters (0 km) and dies away to the NW. What is of more interest is that there are a number of sign changes, so that (for example) changes of opposite sign on the two strainmeters can come from slip over only certain areas on the fault.

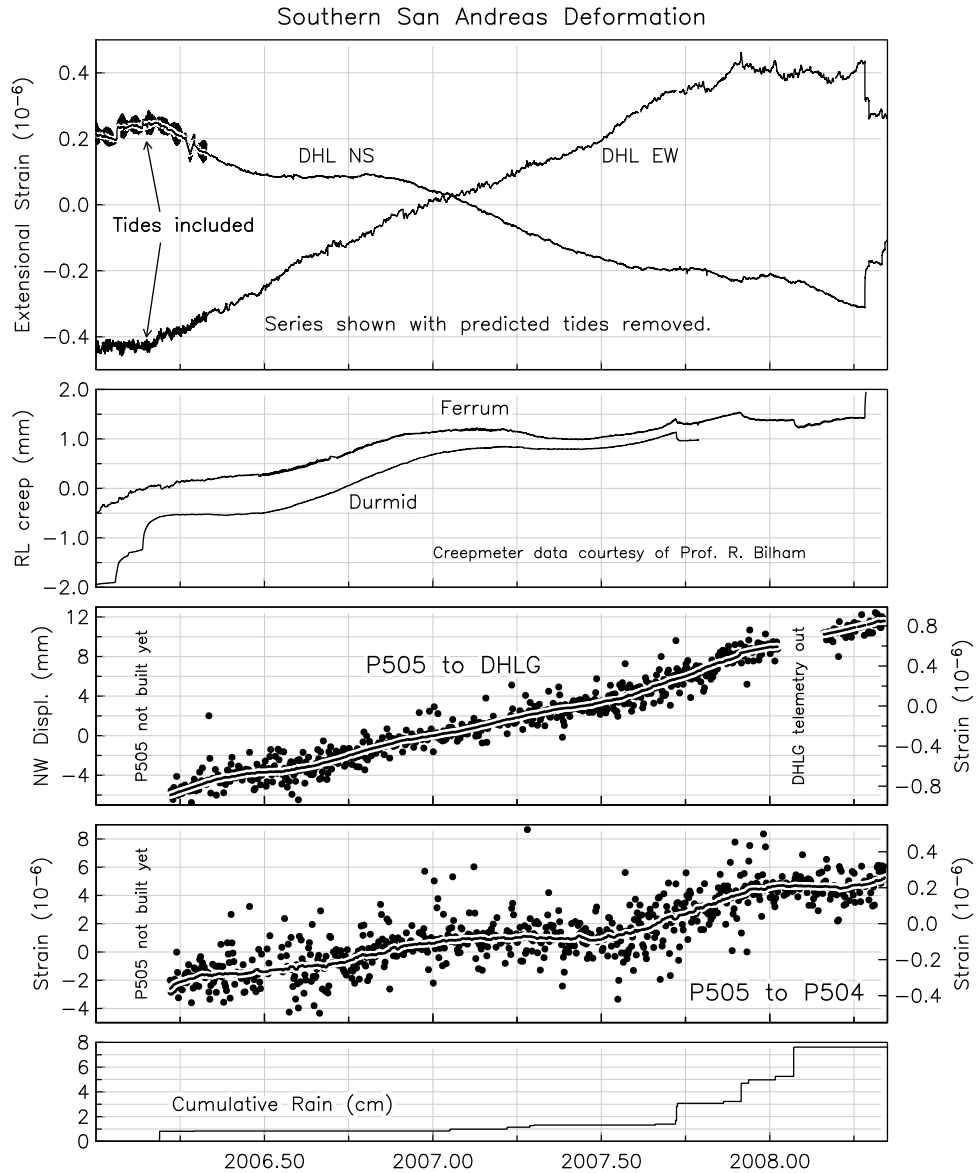


Figure 11

More generally, if we consider the ratio of strain change on two instruments from one sample to the next, each time point for a particular event will allow slip only in particular regions. As the event progresses, these regions will change in shape and location. The problem is then to infer a range of possible solutions, ideally as restrictive a range as possible, from these time-varying regions. This is likely to require additional restrictions, for example that the slipping region remain as compact as possible; this would be analogous to finding a source with minimum moment, an extremal problem that Johnson *et al.* (1994) developed for coseismic slip. Applying a similar constraint to the inversion here is more complex, since it involves a 2-d geometrical minimization; and even with this constraint the solution is unlikely to be unique.

As an elementary example, **Figure 13** shows that for very shallow slip, the ratio of strains is positive for slip NW of the -3 km point, and negative only between -3 and -1 km. Since most of the signals in **Figure 12** show opposite signs, this means that the slip, if shallow, must have been in this region—as

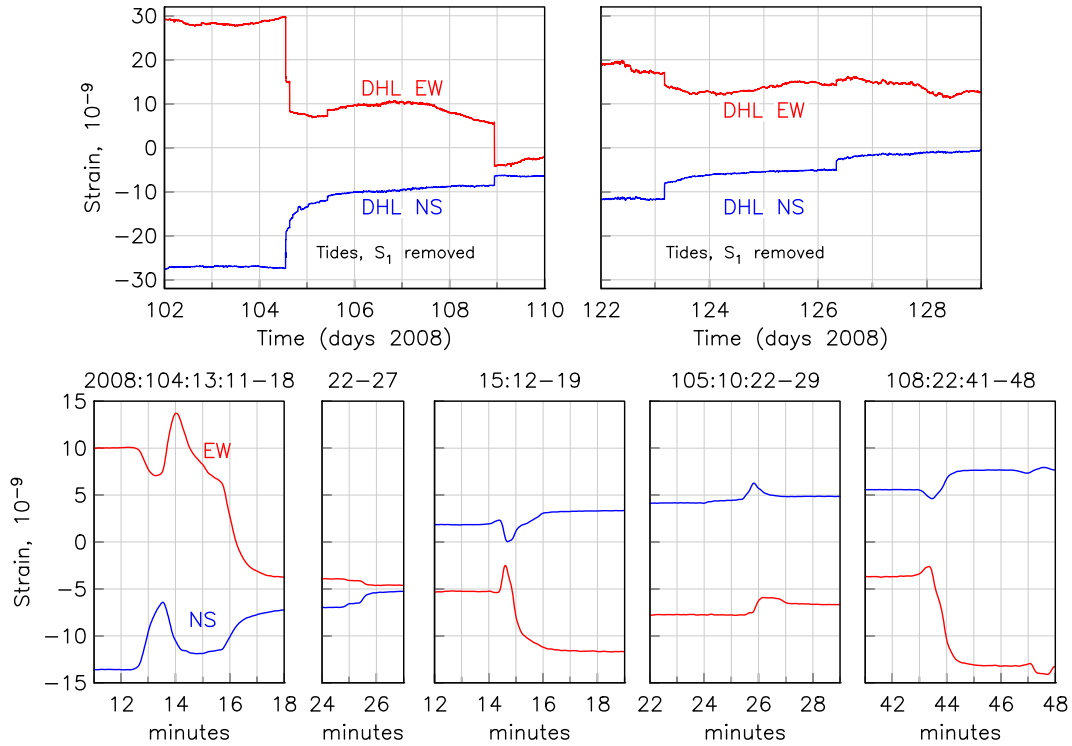


Figure 12: The top two panels show two periods during which the Durmid Hill strainmeters recorded aseismic creep events (data lowpassed with a corner frequency of .005 Hz). The bottom panels show details of the larger creep events for the period 2008:104-105; for all of these the time scale is in minutes, and the data have been lowpassed with a corner frequency of 0.07 Hz to remove microseisms.

well as 10 km away at the Ferrum creepmeter. However, the small event at 2008:105:10:22 (fourth bottom panel of **Figure 12**) must have been NW of -3 km (or, less likely, SE of -1 km).

Some additional constraints on the slip model are available from the creepmeter data (although the timing is less certain, and the data are sampled only every 10 minutes) and also from the absence of a signal on the long-base strainmeters at SCS, on the other side of the Salton Sea; these SCS data limit the total moment release in these events.

3.3. 2009: An Earthquake Swarm near the Southern San Andreas Fault

In 2009 there was seismic activity in the region just south of Bombay Beach: enough activity that it warranted a conference-call meeting of the California Earthquake Prediction Evaluation Council (CEPEC). **Figure 14** and **Figure 15** summarize activity in this region in time and space. **Figure 14** shows the time history since the start of the network, zooming on more recent periods. In each frame, colored symbols identify temporal clusters (red for magnitudes over 3.5), which are seen in the data throughout this period. The start of digital recording around 1980 greatly increased the detection threshold (and the location accuracy); since then, there have been eight clusters. As this figure and **Figure 15** shows, those before 1990 were relatively small (in terms of maximum magnitude) and were located relatively far south of the end of the San Andreas. Since 1999 there have been four clusters, with locations that have, over time, migrated north.

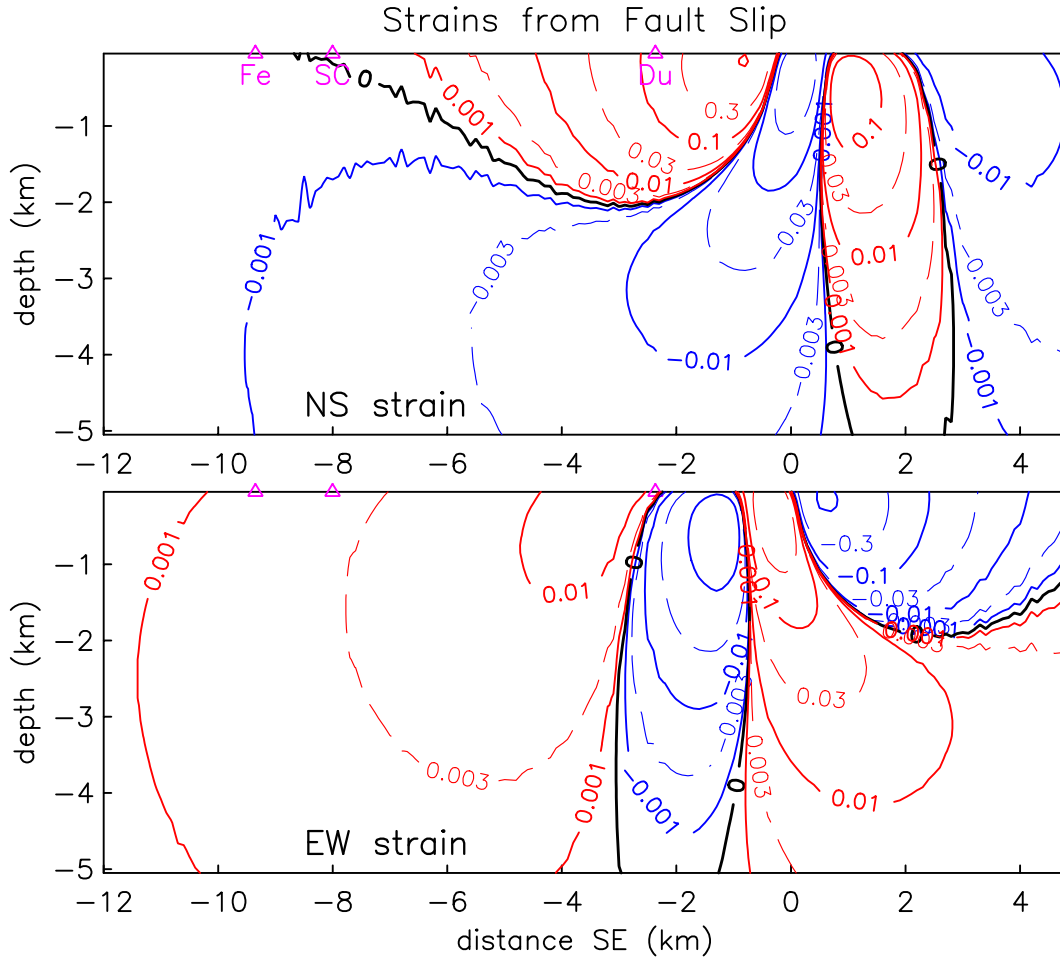


Figure 13: Contours of the Green function for strain from right-lateral strike-slip on a vertical plane coincident with the fault trace. Red is positive, blue negative; amounts are 10^{-9} strain for 1 cm of slip over a patch 100 m square.

The most recent of these clusters began with a swarm of earthquakes on March 21, 2009. On March 23 there was a magnitude 4.8 event at the northernmost edge of what had been observed previously, which was followed by considerable aftershock activity; thanks to the addition of new seismic stations in this area in 2008, this could be followed in detail. The large size of the mainshock (the largest in 50 years), and its proximity to the San Andreas, caused the concern that resulted in the meeting of CEPEC, which suggested issuing an earthquake advisory, since the computations of Agnew and Jones (1991) showed a short-term probability of 5% that this might be a foreshock to a large San Andreas earthquake.

An important source of reassurance during this seismic swarm (not for the first time) was that the laser strainmeters at DHL did not show evidence for any substantially unusual deformation—which, as the previous section has shown, are very sensitive to slip on the San Andreas fault. **Figure 16**, greatly expanded and annotated in some detail, shows the data around the time of the swarm. The NS instrument optics were thrown out of alignment by the largest event but quickly recentered by remote control. It shows a continuation of steady secular strain accumulation, with no obvious effect from the seismicity. The EW instrument had suffered power problems earlier (for reasons unrelated to the shaking, as shown

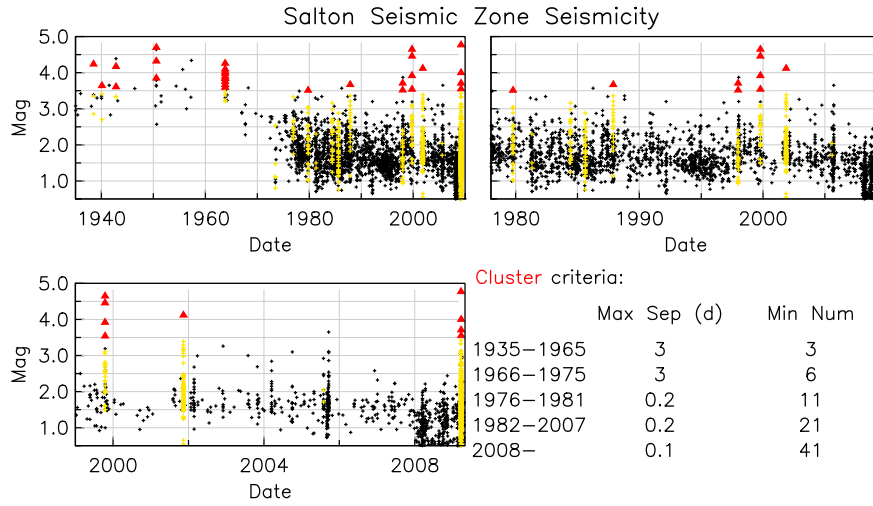


Figure 14

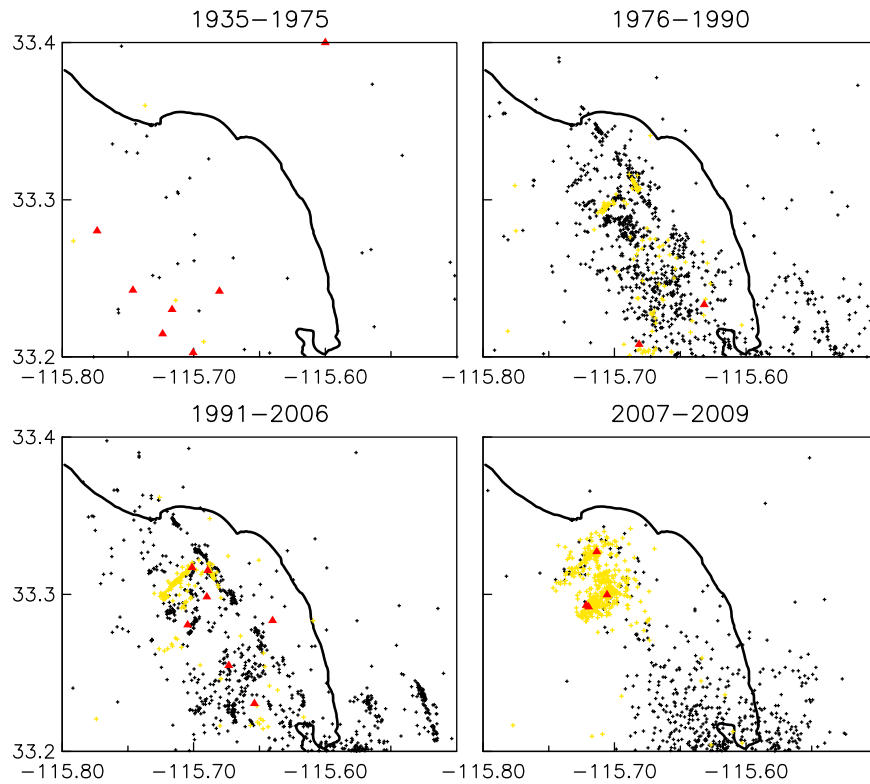


Figure 15

by relative times); fixing this accidentally misaligned the optics of one optical anchor, so the data from this instrument is noisy for about three days. However, when this problem was fixed, the secular rate returned to its previous level.

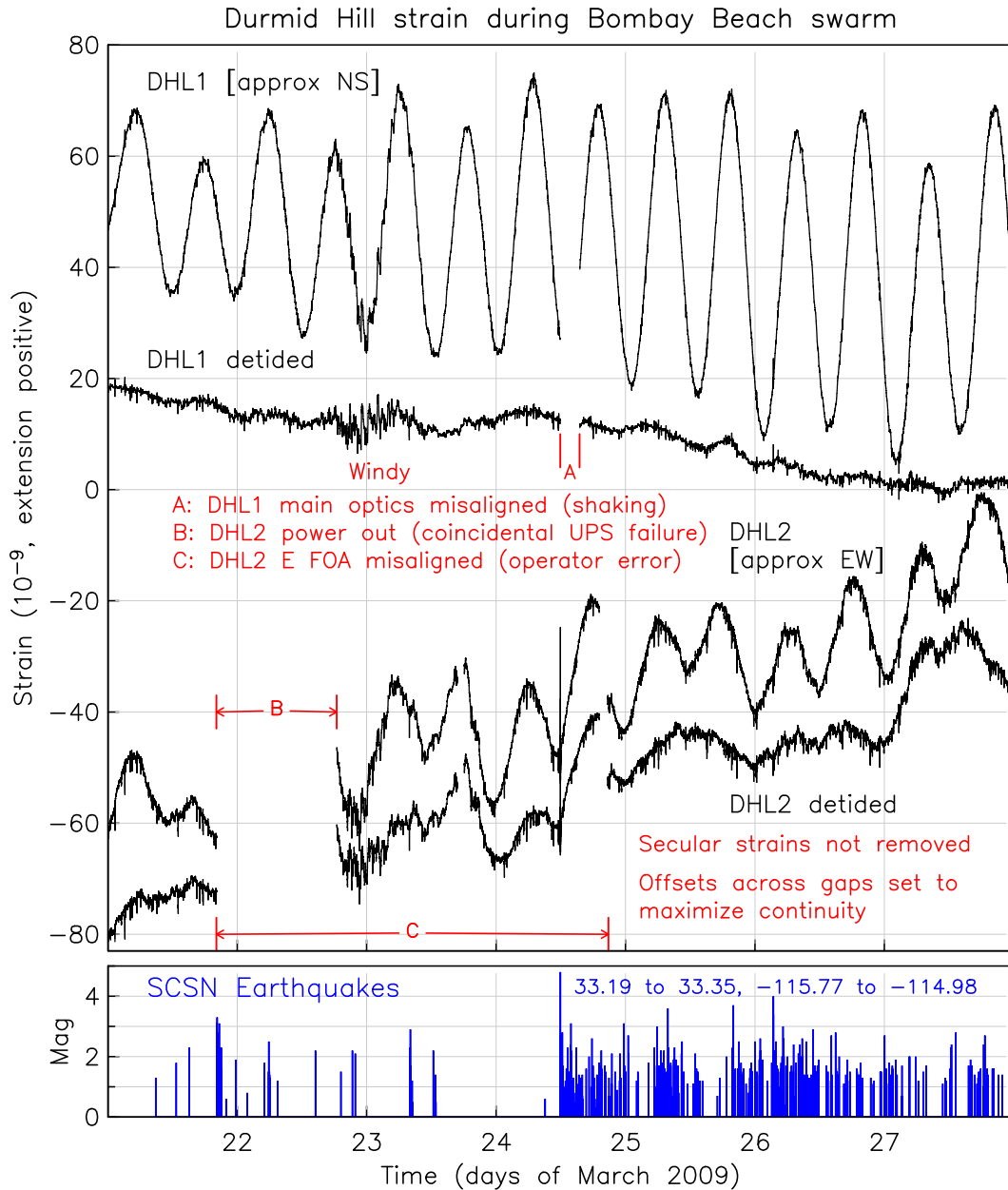


Figure 16

3.4. Long-term Strain Changes at PFO

Figure 17 shows the long-term signals for the NWSE strainmeter at PFO, which was, for most of the time shown, the only well-anchored one. (The NS strainmeter was anchored at one end between 1988 and 1994, and again from 1997 on; the EW instrument has been anchored since 2004.) The “bump” after 1992.5 is postseismic strain from the Landers earthquake; the apparent offset at the earthquake is actually rapid aseismic strain change, starting immediately after the event, and for the first six months increasing roughly as the log of the elapsed time. In late 1992 the strain rate reversed sign; this lasted until 1995; the strain-rate then returned to approximately its pre-earthquake value, though perhaps being somewhat higher. Data (not shown) from the long-base tiltmeter at PFO, though noisier, shows very similar post-

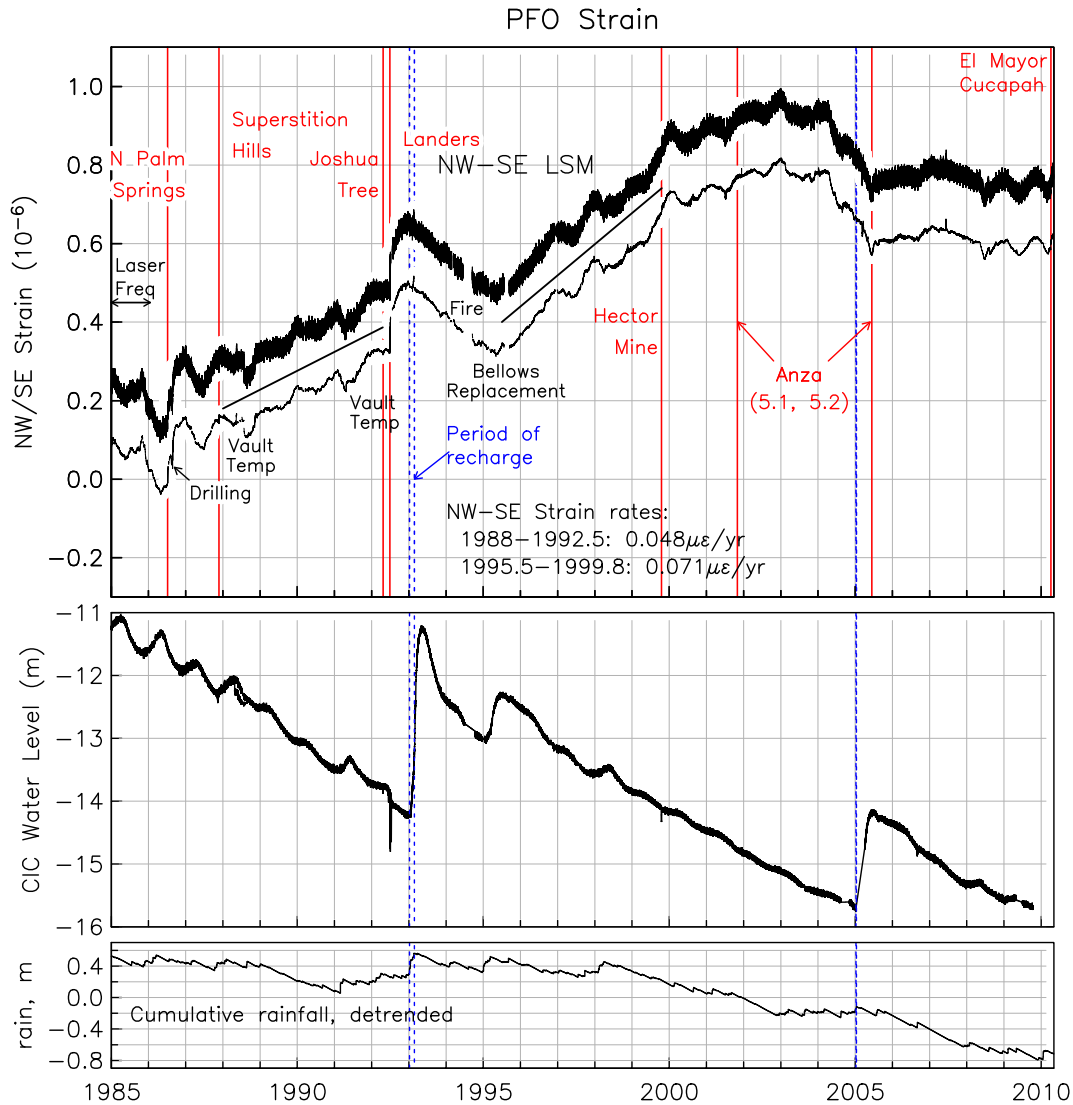


Figure 17

Landers behavior — so this signal is not from just one instrument. Records from monitoring wells at PFO, one of which is shown in **Figure 17**, showed a large change in early 1993 after heavy rains; this did not induce any response in the long-base strainmeter or tiltmeter, ruling out the possibility that the post-seismic signals were caused by local pore-pressure changes, though their cause remains unclear. The 1999 Hector Mine event caused a much smaller and briefer immediate postseismic signal. However, following the Hector Mine shock, the strain rate slowly decreased and by 2004 had again reversed, only to change abruptly, to a rate near zero following the 2005 Anza earthquake, which also produced pronounced short-term and intermediate-term aseismic signals.

The post-2001 changes have been quite dramatic, especially compared with the rather steady accumulation seen for the previous 13 years. While we do not have a well-constrained model for these variations, the results are consistent with slip on faults nearby, and they do not correlate with any fundamental instrumental modifications or changes in operation.

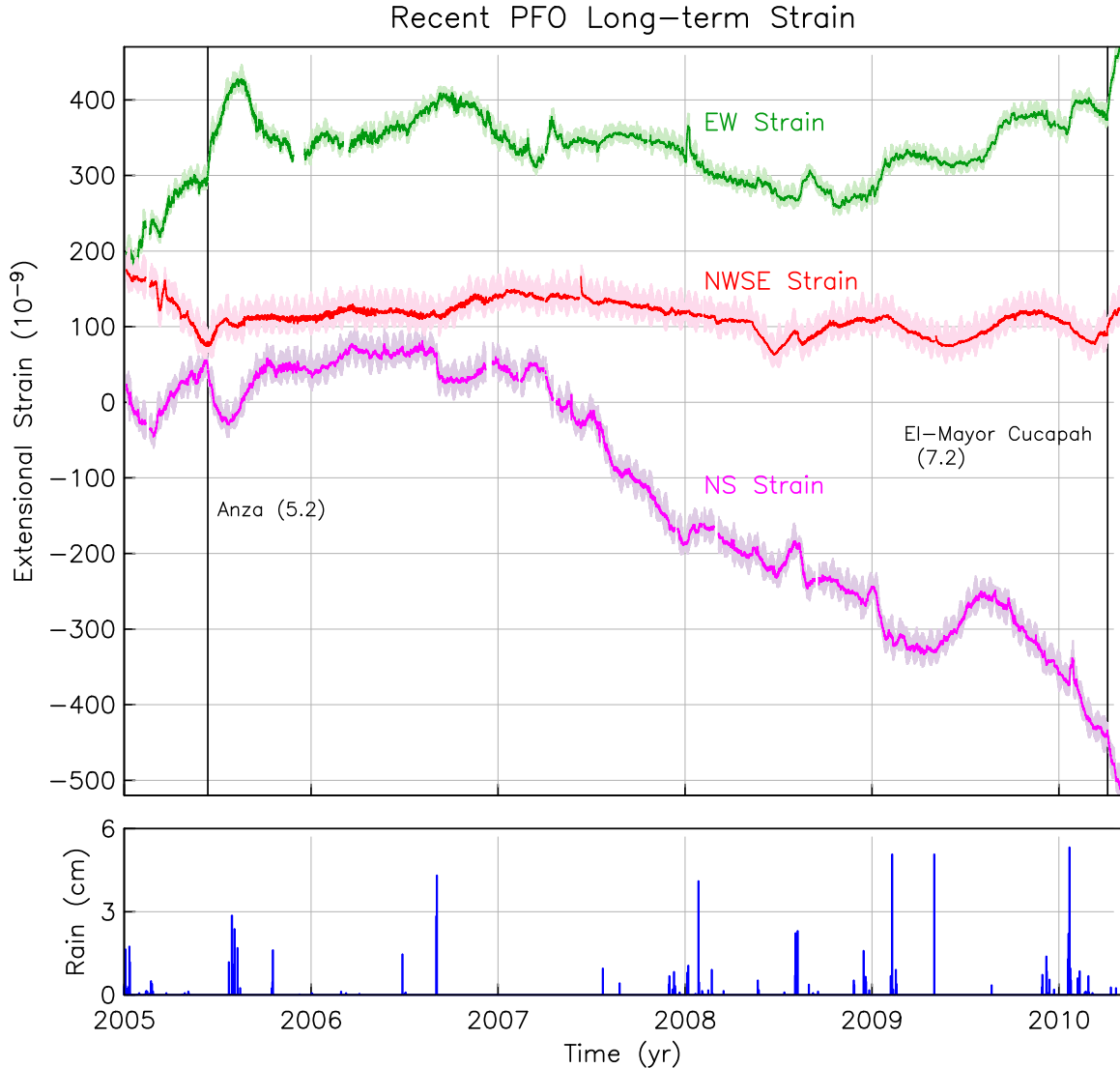


Figure 18: Strain as measured by the three PFO strainmeters from 2005 through the present. For each, the underlying pale color shows the data with the tides present, and the overlying line the data after the tides have been removed. The bottom frame shows the daily rainfall.

Figure 18 is an expanded view of the more recent data, showing the time series for all three of the PFO strainmeters. The EW instrument has been fully anchored during this interval, though it remains somewhat noisier than the NW, probably because the end points are above ground. The NS instrument is anchored only at one end (other activities have had a higher priority for the funding agencies) and is therefore the most susceptible to rain-related noise – the secular rate is probably not correct. There are also variations known to be caused by instrumental effects: for example, the decaying transients on the EW strain in 2007.2 and 2008.0, and on the NWSE at 2007.4, are caused by readjustment of the vault temperatures following extensive power outages or air-conditioner failures.

However, there are some correlated signals that we believe indicate aseismic slip variations on nearby faults. The 2005 Anza earthquake was followed by transients lasting several days on all three instruments, and then by a 6-month signal with opposite sign on the NS and EW sensors, and a much

smaller variation on the NWSE: this is the signature that would be expected from slip on the San Jacinto fault. It should be noted that these three instruments have no elements in common. A somewhat similar variation, with the NS and EW systems showing opposite signals, started at the beginning of 2009; although this looks somewhat like an annual variation, the period is shorter than this, and we know of no changes to the instruments that would suddenly have made them more temperature sensitive.

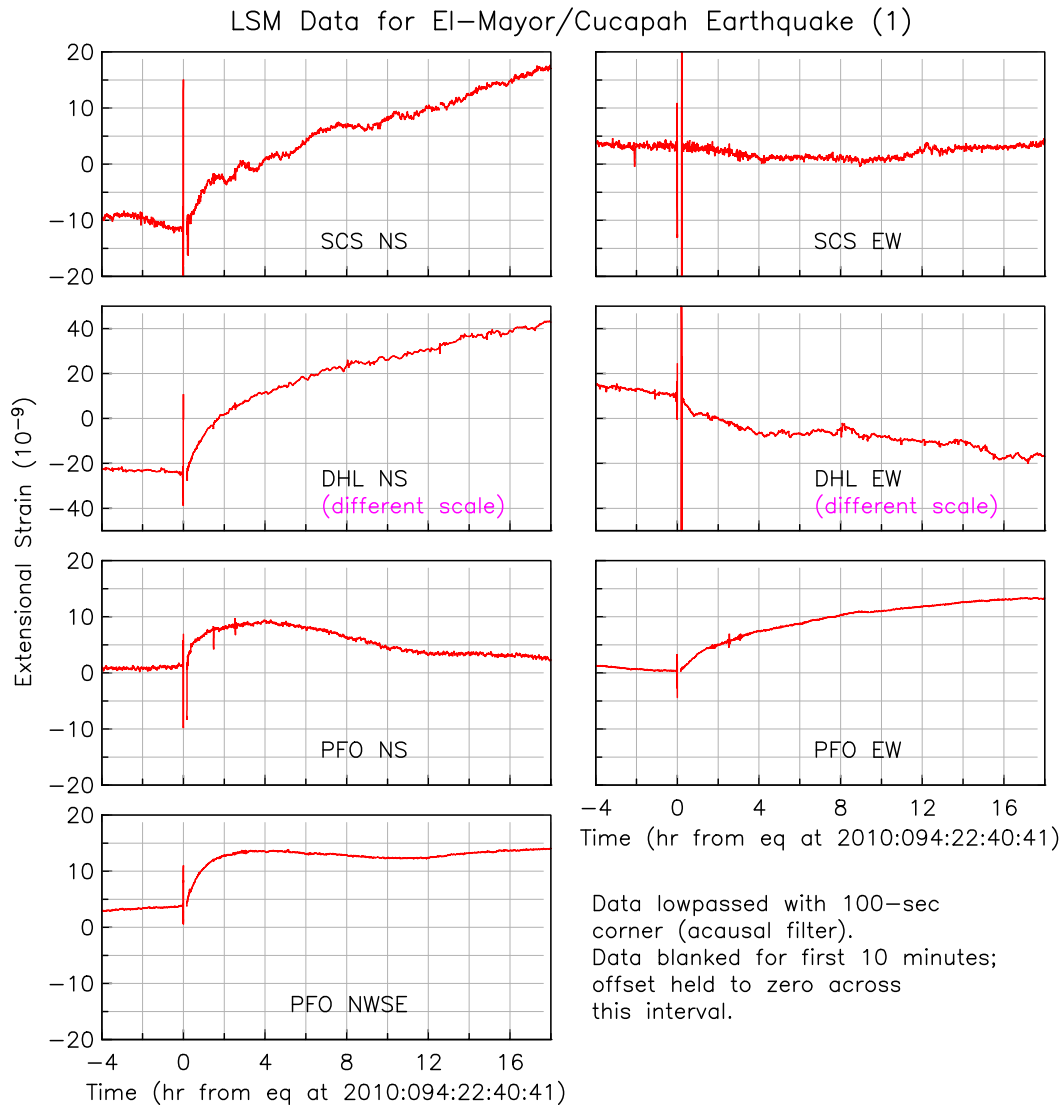


Figure 19

3.5. 2010: Strain Changes From the El-Mayor Cucapah Earthquake

Although it falls just outside the time range of this report, we felt it appropriate to present data from the El-Mayor/Cucapah earthquake of April 4, 2010 (hereafter the EMC earthquake), located in Baja California in the Cucapah mountains that bound the Mexicali Valley to the West. A relatively fresh scarp found by Mueller and Rockwell (1995) along the western side of the mountains, called the Laguna Salada fault, is generally assumed to be associated with a large earthquake (magnitude 7.2) in February 1892; the intensity reports are at least consistent with such a location (Hough and Elliot 2004). Just over 118 years

of strain; in the plots we have set the offset to be zero across this gap so that we can best show other changes. Since much more information on coseismic behavior is available from seismic, GPS, and InSAR, the loss of this information while unfortunate, is not fatal. We do have reliable estimates of coseismic offsets from the EW longbase tiltmeter at PFO, and from the more distant strainmeters in Los Angeles and Cholame.

After this interruption the strainmeters give a continuous record of even small deformations. The plot shows the result of lowpassing the original 1-Hz data (filter corner at 100 s) to remove the seismic coda. When this is done these records show immediate, relatively smooth, strain changes at rates much higher than are observed at any other time. Such postseismic motions, if caused by afterslip on the fault, provide important constraints on the laws governing fault slip (Larson and Miyazaki 2008; Fukuda *et al.* 2009).

The data in **Figure 19** and **Figure 20** suggest, however, a more complex picture than simple afterslip on the fault that caused the EMC earthquake. Table 1 gives the predicted coseismic strains, and some ratios between them, for a simple uniform-slip model. For the strains at SCS, these ratios are in reasonable agreement with what is observed. In particular, the model predicts that the ratio between EW and NS strains is small, something that the data also demonstrate, as the signal on the EW strain data is very small. A more detailed examination of the EW/NS ratio as a function of position along the fault shows that the smaller values of this ratio occur farther south on the fault, which would imply that the afterslip may be more in the region of the epicenter than at the northern termination of the rupture. As usual, the postseismic deformations are much too large to be caused by the observed aftershocks.

Table 1: Model Coseismic Strains

	NS	EW	NW	EW/NS	NW/NS
Model Coseismic Strains					
SCS	314	46.4	—	0.15	—
DHL	355	-40.8	—	-0.12	—
PFO	9.4	31.0	55.7	3.3	5.9

We therefore assume, as a first approximation, that the SCS NS data in **Figure 19** and **Figure 20** represent the time history of afterslip on the fault that caused the mainshock. If that were the only process at work, we would expect all the other strainmeter records to look like scaled versions of this time series; that these records do not look like this suggests other sources of strain were triggered by the mainshock.

Looking first at the DHL data, we see a much larger and faster response on the NS, even though the model predicts similar responses for the SCS and DHL NS strains. The ratio of EW to NS response is also much larger than predicted by the model. And, we observe several small steps in these series that are not seen elsewhere (one large event is identified in the figure). Our tentative explanation for all this is that the instruments are recording, not just strains from the EMC earthquake, but also signals from aseismic slip induced on the San Andreas fault, which is only 1.5 km away at the closest. We have observed similar slip events on DHL strainmeters, without accompanying seismic events, in 1997, 1999, 2003, 2006, and 2008; the last was the largest episode of aseismic strain so far observed, and was also recorded on nearby creepmeters. Further, as discussed earlier, seismic swarms have occurred nearby, on the northern end of the Brawley seismic zone, but none of these has been associated with any significant strain change.

The idea that the strain signals at DHL were caused in part by near-surface slip on the San Andreas fault is supported by results from Prof. Bilham’s creepmeter array; the instrument at Salt Creek, 9 km NW of DHL, showed a few mm of creep coincident with the EMC earthquake. Triggered surface creep has been observed on the San Andreas and other faults of the Salton Trough before; the Superstition Hills

fault, site of a large creep event in 2006 (Wei *et al.* 2009) showed large surface creep triggered by the EMC earthquake. Triggered creep is thus quite plausible as an explanation of the signals seen at DHL, but that does not make them any less interesting, since they provide a level of resolution in time and signal level not achieved by any of the other data available.

Even more interesting are the signals from PFO, which is closest to the San Jacinto fault. All three strainmeters there start by showing postseismic strains that are roughly consistent, in size and shape, with their source being afterslip from the EMC fault: the signals are of the same sign, and larger on the NWSE and the EW than on the NS. However, as **Figure 20** makes especially clear, the strains over the first month after this earthquake do not fit this pattern at all: instead, the NS and EW show trends of about the same size but opposite sign, while the NWSE shows less change; we also observe a significant change in trend on the long fluid tiltmeter. Slip on the San Jacinto fault would produce exactly this pattern: for example, the NWSE, being parallel to this fault, is the least sensitive to slip on it. Although the trends on the PFO instruments seem to be decreasing in rate, they are doing so only with a long time constant; as we described above, a similar pattern followed the 2005 Anza earthquake. If these strains indicates triggered deep-slip on the San Jacinto fault, such slip is continuing at the time of this writing.

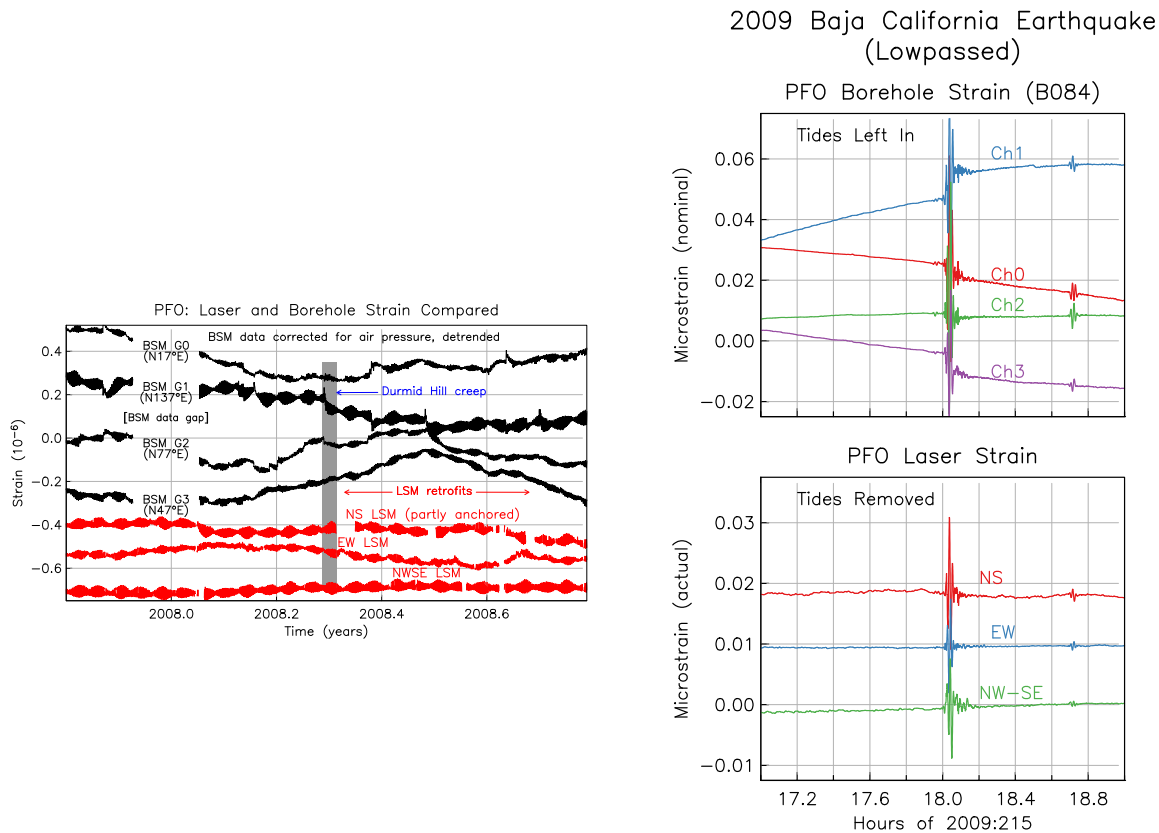


Figure 21

3.6. Instrument Comparison: Longbase and Borehole Strainmeters

As an example of the sort of instrument comparison possible at PFO we show some results from the PBO borehole strainmeters and the longbase laser strainmeters; **Figure 21** presents a representative year of data from the PBO BSM at PFO, starting 13 months after it was installed. Each BSM has four sensors, three measuring internal strain at angles of 60°, and a fourth (redundant sensor) to make a right-angled pair for instrument validation. We have removed a slope and best-fitting exponential from each BSM

channel, since at the longest periods (and at this stage of the installation) these trends give strain rates about 100 times the tectonic rate; we have also removed the best-fitting air-pressure response, which for these BSM's is substantial. The plot also shows data from the three laser strainmeters, which surround the BSM location. The NS laser instrument is not anchored to depth at one end, and so is noisier than the other two. It is clear that for periods longer than a week or two, the LSM's have better stability; the BSM data also show a number of events, some correlated between different sensors, which, not being visible on the LSM's, cannot be coming from the earth on the scale of 1 km. This plot also spans the time of a prolonged San Andreas fault aseismic-slip episode detected by the DHL longbase strainmeters in 2008; the absence of a signal at PFO confirms that the slip was not widespread.

Another comparison between borehole and longbase strain was provided by an M_w 6.9 earthquake in the Gulf of California (610 km away) on 2009:215. The size, proximity, and radiation pattern of this event produced dynamic strains of about $\pm 10^{-6}$ peak to peak. Strains this large are relatively rare, with only three other examples in the last five years; these were the first large dynamic strains since the installation of the PBO BSM's in the Anza area. Most of the Anza BSM's showed offsets from this earthquake. **Figure 21** shows the BSM and LSM data from PFO, lowpassed to reduce the size of the surface waves, though the mainshock and an aftershock are still visible. None of the three LSM's show any offsets; for the best of the LSM records (the NW-SE) the upper limit on a possible step is 10^{-10} strain, a few percent of the offsets seen in the BSM data.

Since the BSM at PFO is embedded in the rock bounded by the LSM's, these data imply that the BSM offsets are of very local origin, which brings into question the offsets seen at other locations. Localized hydrological changes, which are often triggered by large dynamic strains, might be a source, though the pore-pressure record at the BSM shows no changes (to within 5 Pa). These recordings imply that co-seismic and postseismic strain data from BSM's subject to large dynamic strains must be used only with some caution.

4. Instrument and Site Improvements

With NSF instrumentation-support during this grant period we have made a number of upgrades to the laser strainmeters at PFO and DHL, in order to make higher quality deformation data available to researchers from sites that, because of their long time history, provide a particularly valuable baseline. Many of these upgrades involved installing, at these older instruments, improvements that had been developed in the course of building newer systems, particularly the one at Yucca Mountain, for which we had much more severe restrictions on access than usual, but also a budget that permitted some degree of development work.

4.1. Instrument Improvements

4.1.1. Strainmeter Datalogger/Controller

We introduced several special-purpose controller/dataloggers at PFO. The first unit, servicing 128 signal-channels, permitted recording and active interrogation of all the low-frequency instruments at the site. We subsequently introduced 32-channel systems at each of the three strainmeters at PFO; these systems provide recording and network-interrogation of signals, and also remote control of the following:

Laser-beam steering. This control system, included in the datalogger, keeps laser beam optimally aligned over the half-mile length of the instruments.

Laser Control. With this we can remotely monitor the frequency stability and laser performance (the best warning of incipient degradation), and also more quickly relock the laser when needed.

Automated Vacuum Control. Together with a new-pumping system (discussed next) this system provides the means to bring the system back up whenever power restored following an outage, without any loss of vacuum. This also gives us remote operation and diagnosis of the vacuum pumps and valving.

4.1.2. Conversion to Continuous Vacuum Pumping

Beginning in late 2006, we augmented the vacuum-pumping housing and hardware to include low-capacity pumps meant to run continuously. With the control valves for this tied to the datalogger/controller, the end-to-end vacuum pipe can be maintained at very low pressures and isolated during power failures (when the pumps do not operate), and sustained at operational vacuum levels until such time as the power is restored.

4.1.3. Improved Temperature Control

Despite first-order immunity to temperature changes, at the low noise levels now being achieved with the strainmeters some thermal effects were evident. Heat-pump air conditioners are only meant to do a fair job of regulating temperature, and, of course, do not run during power outages. To improve on this we added active thermal-control systems for the optics tables, using pairs of thermoelectric modules (TEM) mounted in the walls of the instrument enclosures, and controlled by a programmable microprocessor. This system provides two important advantages:

- The active control isolates the temperature inside from that outside as a passive system cannot, making the inside temperature immune from (for example) fluctuations when the end building is visited. **Figure 22** shows an example, for the new strainmeter in Glendale: once the controller is on, the rms temperature variation on the optics table is reduced to only 0.02°C.
- This control runs on separate batteries, and so continues to function throughout power failures, maintaining fully regulated temperatures.

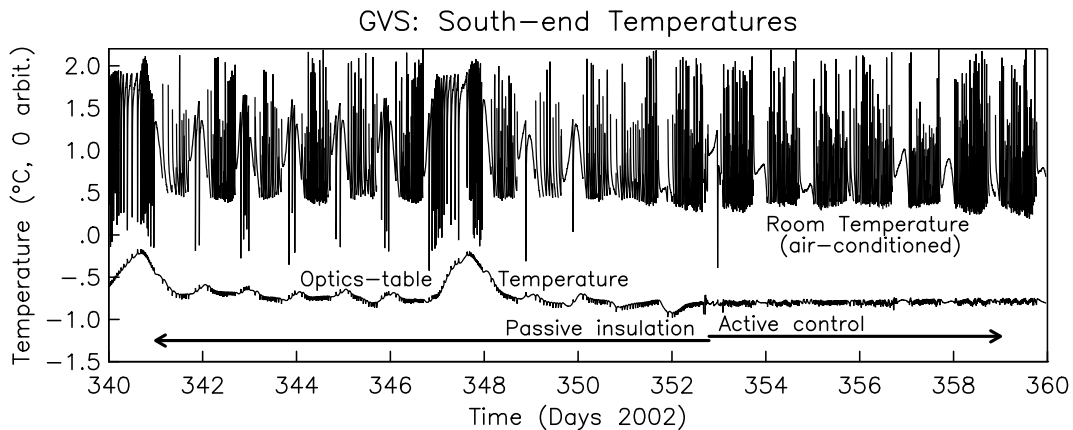


Figure 22

In response to maintenance needs: the heat-pump systems used to control temperature in the strainmeter end buildings were on average 12 years old, well past their nominal 7-year lifetime (at which point they all begin to have troubles); because we function with only a few back-up units, the irreparable failure of several in-use air conditioners in 2007, left us in a precarious situation. We purchased 6 new systems (which include programmable-control), one for each end of three of the four strainmeters, and retrofitted the buildings for their installation.

4.1.4. Optical Anchor pathlength modulators.

We added micro-displacement forcing systems to all the optical anchors to modulate the optical-fringe signal every few minutes: the only way to provide the information needed for the electronics to track the signals as the optical alignment varies with time.

4.1.5. High Dynamic Range Fringe Counters

Our older electronics were all designed to operate with a 12-bit recorder. The large digitizing step size associated with these systems meant that we had very limited dynamic range, and signals from local or large regional earthquakes sometimes saturated the recording system. The new dataloggers use 16-bit digitizers (with correspondingly smaller step-size), allowing us to reduce this problem by installing new high-dynamic range counters, all with means for remote control, so we can reset parameters during operation.

4.1.6. Uninterruptible Power Supplies

We purchased five UPS's with remote-control capabilities, and which can send diagnostic signals to the datalogger, in order to protect the recordings against short power outages. Short power failures are very common; at PFO we have a standby-generator for longer ones (the existing less-than reliable generator, installed in the mid 1970's, is currently being replaced under USGS/ARRA support). The combination of the two systems provides full protection for power loss.

With the availability of modular UPS systems to maintain power to the optics and electronics, automated and battery-powered instrument temperature regulation, and self-sustaining vacuum levels, the strainmeters are now able to continue recording unperturbed through all but extended power outages, greatly improving the long-term observations.

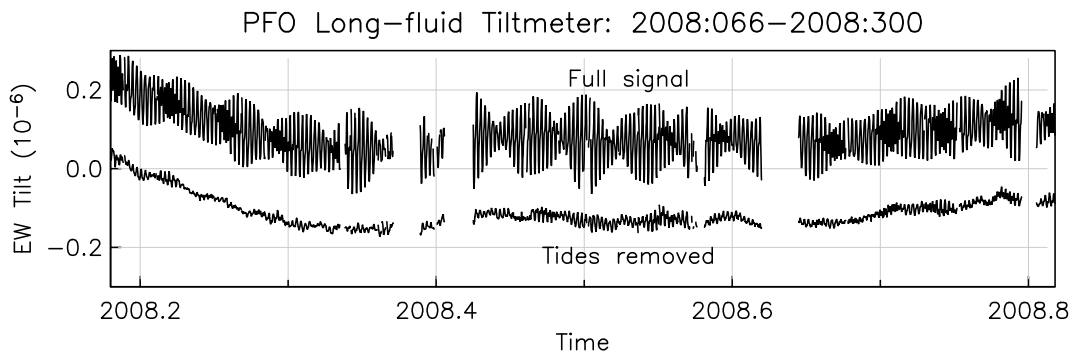


Figure 23

4.2. Tiltmeter Reconstruction

In the 1980's we constructed two long-base tiltmeters at PFO, with USGS and NSF support. These have given excellent records, for example showing the same post-Landers transient in tilt that **Figure 17** shows in strain. Unfortunately, a severe lightning storm in mid-2004 destroyed much of their electronics. Rebuilding was slowed by higher-priority tasks and the 18-month illness of the technician most familiar with the system; but over the last few years these have been reconstructed. **Figure 23** shows early data from the rebuilt EW instrument.

5. Data Handling

Over the last few years there has been increasing interest in the accessibility of the longbase strainmeter data. In the past, we have handled data from PFO and DHL as is usual for a research project: data were made available to the community through publication of the scientific results, and by direct collaboration with other researchers who might be interested in them; for PFO data examples include Abercrombie *et al.* (1995), Gomberg and Agnew (1996) Hart *et al.* (1996), and Elkhoury *et al.* (2006). In addition, we have made results available as promptly as possible whenever something has happened to raise the possibility of aseismic deformations leading to large earthquakes: for example, the Landers earthquake, or swarms near Durmid Hill. However, we have not routinely provided final data for general use; neither PFO nor DHL was funded at a level that could support this.

There is now much more of an expectation that data should be, as much as possible, available online with little delay: a valuable goal, but not without costs. The cost of providing strainmeter data in usable form is relatively high (compared to seismic or GPS data) because these data are relatively unfamiliar to most solid-earth geophysicists, relatively unstructured (compared with, say GPS RINEX), and relatively difficult to interpret because we know so little about aseismic sources of strain and there are so many possible sources of noise. Getting the most science from the data requires a fair degree of familiarity with the sensor.

Improving data access requires investment in three areas: (1) upgrading the hardware (datalogging and telemetry) to make the raw data promptly and routinely available, (2) improving the software for data handling, and (3) upgrades to equipment to make the data as trouble-free as possible. As described in the previous section, we have been able to use other funds to make progress in all three areas.

Most of the research community is best served by downloadable files of final data, regularly updated. For research purposes we updated data only occasionally (in part because of the personnel issues described above); to provide regular updates at an acceptable level of effort has required additional software development to process the raw data, assemble it into files for editing, organize the edits, and produce the final results—also mundane, but not simple (indeed, still being worked on). All of this development was supported by the PBO, for which there is a clear expectation of regularly-updated data. At this time both the PFO and DHL data are being processed using these packages, so that all data are being handled in the same way.

With other funding we have spent considerable effort to help build a community of users for strain data, co-teaching in two workshops organized by UNAVCO in 2008 and 2009, and documenting and making available our processing software (<http://igppweb.ucsd.edu/~agnew/piasd>).

Data from the laser strainmeters at PFO and DHL are now being made available to the research community by providing files to the NCEDC in the same formats as PBO; that is, as fully-corrected and edited data in the XML format used by PBO, with a latency of no more than six months; we are also providing, every two weeks, up-to-the-moment preliminarily edited-versions of the signals. We are committed to making older data available on request.

In addition, plots of raw data continue to be available in real time through the RoadNet system; see http://mercali.ucsd.edu/waveform.cgi?n=n&level=0&mode=sta&db0=db_pfo; click on channel 3, for the main strainmeter signals at each site; for the NS LSM at DHL, the station name is DHL1; for the NS LSM at PFO PFO4; for the EW LSM, PFO5; and for the NW LSM, PFO6. (None of these are 'corrected' strain.)

References

- R. E. Abercrombie, D. C. Agnew, and F. K. Wyatt, "Testing a model of earthquake nucleation," *Bull. Seismol. Soc. Amer.*, 85, pp. 1873-1878 (1995).
- D. C. Agnew and L. M. Jones, "Prediction probabilities from foreshocks," *J. Geophys. Res.*, 96, pp. 11959-11971 (1991).
- C. R. Allen, M. Wyss, J. N. Brune, A. Grantz, and R. E. Wallace, "Displacement on the Imperial, Superstition Hills, and San Andreas faults triggered by the Borrego Mountain earthquake, in The Borrego Mountain Earthquake of April 9, 1968," *U. S. Geol. Surv. Prof. Pap.*, 787, pp. 87-104 (1972).
- G. Anderson, D. C. Agnew, and H. O. Johnson, "Salton Trough regional deformation estimated from combined trilateration and survey-mode GPS data," *Bull. Seismol. Soc. Amer.*, 93, pp. 2402-2414 (2003).
- E. A. Babcock, "Structural geology and geophysics of the Durmid area, Imperial Valley, California," Ph.D Thesis, University of California Riverside (1969).
- R. Bilham, N. Suszek, and S. Pinkney, "California creepmeters," *Seismol. Res. Lett.*, 75, pp. 481-492 (2004).
- J. R. Brown, D. R. Shelly, A. Aguiar, and G. C. Beroza, "Triggered tremor on the San Jacinto fault from the 3 August 2009 Mw 6.9 Gulf of California earthquake," Annual Meeting Reports, pp. 1-095, SCEC (2009).
- R. Bürgmann, "Transpression along the southern San Andreas Fault, Durmid Hill," *Tectonics*, 10, pp. 1152-1163 (1991).
- J. E. Elkhoury, E. E. Brodsky, and D. C. Agnew, "Seismic waves increase permeability," *Nature*, 441, pp. 1135-1138 (2006).
- K. F. Evans, R. O. Burford, and G. C. P. King, "Propagating episodic creep and the aseismic slip behavior of the Calaveras Fault north of Hollister, California," *J. Geophys. Res.*, 86, pp. 3721-3735 (1981).
- N. P. Fay and E. D. Humphreys, "Fault slip rates, effects of elastic heterogeneity on geodetic data, and the strength of the lower crust in the Salton Trough region, southern California," *J. Geophys. Res.*, 110, p. B09401 (2005).
- Y. Fialko, "Interseismic strain accumulation and the earthquake potential on the southern San Andreas fault system," *Nature*, 441, pp. 1135-1138 (2006).
- J. Fletcher, T. Fumal, H.-P. Liu, and J. C. Carroll, "Near-surface velocities and attenuation at two boreholes near Anza, California from logging data," *Bull. Seismol. Soc. Amer.*, 80, pp. 807-831 (1990).
- J. Fukuda, K. Johnson, K. M. Larson, and S. Miyazaki, "Friction parameters inferred from the early stages of afterslip following the 2003 Tokachi-oki earthquake," *J. Geophys. Res.*, 114, p. B04412 (2009).
- M. T. Gladwin, R. L. Gwyther, R. H. G. Hart, and K. S. Breckenridge, "Measurements of the strain field associated with episodic creep events on the San Andreas fault at San Juan Bautista, California," *J. Geophys. Res.*, 99, pp. 4559-4565 (1994).
- J. Gomberg and D. C. Agnew, "The accuracy of seismic estimates of dynamic strains: an evaluation using strainmeter and seismometer data from Piñon Flat Observatory, California," *Bull. Seismol. Soc. Amer.*, 86, pp. 212-220 (1996).

- J. Gomberg, J. L. Rubinstein, Z. Peng, K. C. Creager, J. E. Vidale, and P. Bodin, "Widespread triggering of nonvolcanic tremor in California," *Science*, 319, p. 173 (2008).
- N. Goultly and R. Gilman, "Repeated creep events on the San Andreas Fault near Parkfield, California, recorded by a strainmeter array," *J. Geophys. Res.*, 83, pp. 5415-5419 (1978).
- R. H. G. Hart, M. T. Gladwin, R. L. Gwyther, D. C. Agnew, and F. K. Wyatt, "Tidal calibration of borehole strainmeters: removing the effects of local inhomogeneity," *J. Geophys. Res.*, 101, pp. 25553-25571 (1996).
- S. E. Hough and A. Elliot, "Revisiting the 23 February 1892 Laguna Salada earthquake," *Bull. Seism. Soc. Am.*, 94, pp. 1571-1578 (2004).
- K. W. Hudnut, L. Seeber, and L. Pacheco, "Cross-fault triggering in the November 1987 Superstition Hills earthquake sequence, southern California," *Geophys. Res. Lett.*, 16, pp. 199-202 (1989).
- S. Ide, G. C. Beroza, D. R. Shelly, and T. Uchide, "A scaling law for slow earthquakes," *Nature*, 447, pp. 76-79 (2007).
- H. Johnson, F. Wyatt, and D. C. Agnew, "Present-day crustal deformation in southern California," *J. Geophys. Res.*, 99, pp. 23951-23974 (1994).
- H. O. Johnson, D. C. Agnew, and K. Hudnut, "Extremal bounds on earthquake moment from geodetic data: application to the Landers earthquake," *Bull. Seismol. Soc. Amer.*, 84, pp. 660-667 (1994).
- L. M. Jones, K. E. Sieh, D. Agnew, C. Allen, R. Bilham, M. Ghilarducci, B. Hager, E. Hauksson, K. Hudnut, D. Jackson, and A. Sylvester, "Short-Term Earthquake Hazard Assessment for the Southern San Andreas Fault, Southern California," USGS Open-File Report 91-32, U. S. Geological Survey (1991).
- G. C. P. King, R. G. Bilham, J. W. Campbell, and D. P. McKenzie, "Detection of elastic strainfields caused by fault creep events in Iran," *Nature*, 253, pp. 420-423 (1975).
- K. M. Larson and S. Miyazaki, "Resolving static offsets from high-rate GPS data: the 2003 Tokachi-oki earthquake," *Earth Plan. Space*, 60, pp. 801-808 (2008).
- G. Lin, P. M. Shearer, and E. Hauksson, "Applying a three-dimensional velocity model, waveform cross correlation, and cluster analysis to locate southern California seismicity from 1981 to 2005," *J. Geophys. Res.*, 112, p. B12309 (2007).
- A. T. Linde, M. T. Gladwin, M. J. S. Johnston, and R. L. Gwyther, "A slow earthquake sequence on the San Andreas fault," *Nature*, 383, pp. 65-68 (1996).
- R. B. Lohman and J. J. McGuire, "Earthquake swarms driven by aseismic creep in the Salton Trough, California," *J. Geophys. Res.*, 112, p. B04405 (2007).
- J. Louie, C. R. Allen, D. C. Johnson, S. N. Cohen, and P. C. Haase, "Fault slip in Southern California," *Bull. Seismol. Soc. Amer.*, 75, pp. 811-833 (1985).
- S. Lyons and D. Sandwell, "Fault creep along the southern San Andreas from interferometric synthetic aperture radar, permanent scatterers, and stacking," *J. Geophys. Res.*, 108, pp. ETG 11-1-ETG 11-24 (2003).
- R. McCaffrey, "Block kinematics of the Pacific/North America plate boundary in the southwestern United States from inversion of GPS, seismological, and geologic data," *J. Geophys. Res.*, 110, p. B07401 (2005).

- B. J. Meade and B. H. Hager, "Block models of crustal motion in southern California constrained by GPS measurements," *J. Geophys. Res.*, 110, p. B03403 (2005).
- K. J. Mueller and T. F. Rockwell, "Late Quaternary activity of the Laguna Salada fault in northern Baja California, Mexico," *Geol. Soc. Amer. Bull.*, 107, pp. 8-18 (1995).
- S. J. Radzevicius and G. L. Pavlis, "High-frequency reflections in granite: Delineation of the weathering front in granodiorite at Piñon Flat, California," *Geophysics*, 64, pp. 1828-1835 (1999).
- D. R. Shelly, G. C. Beroza, and S. Ide, "Non-volcanic tremor and low-frequency earthquake swarms," *Nature*, 446, pp. 305-307 (2007).
- K. E. Sieh and P. L. Williams, "Behavior of the southernmost San Andreas fault during the past 300 years," *J. Geophys. Res.*, 95, pp. 6629-6645 (1990).
- R. Uhrhammer, L. S. Gee, M. Murray, D. Dreger, and B. Romanowicz, "The Mw 5.1 San Bautista, California Earthquake of 12 August 1998," *Seismol. Res. Lett.*, 70, pp. 10-18 (1999).
- M. Wei, D. Sandwell, and Y. Fialko, "A silent M_w 4.7 slip event of October 2006 on the Superstition Hills fault, southern California," *J. Geophys. Res.*, 114 (2009).
- R. L. Wesson, "Dynamics of fault creep," *J. Geophys. Res.*, 93, pp. 8929-8951 (1988).
- P. L. Williams, S. F. McGill, K. E. Sieh, C. R. Allen, and J. N. Louie, "Triggered slip along the San Andreas fault after the 8 July 1986 North Palm Springs earthquake," *Bull. Seismol. Soc. Amer.*, 78, pp. 1112-1122 (1988).

Bibliography of Publications

Agnew, D. C. (2007). Before PBO: an overview of continuous strain and tilt measurements in the United States, *J. Geodetic Soc. Japan*, **53**, 157-182.

Tamura, Y., and D. C. Agnew (2008). *Baytap08 Users Manual*, SIO Technical Report: <http://repositories.cdlib.org/sio/techreport/82/>, Scripps Institution of Oceanography.